

Three-dimensional induction of dorsal, intermediate and ventral spinal cord tissues from human pluripotent stem cells

Takenori Ogura^{1,2,*}, Hideya Sakaguchi^{1,*‡}, Susumu Miyamoto² and Jun Takahashi^{1,2,‡}

ABSTRACT

The spinal cord contains more than 20 distinct subclasses of neurons that form well-organized neural circuits capable of sensing the environment and generating motor behavior. Although recent studies have described the efficient *in vitro* generation of spinal motor neurons, the induction of the spinal cord as a whole tissue has not been achieved. In the present study, we demonstrate three-dimensional (3D) induction of dorsal spinal cord-like tissues from human pluripotent stem cells. Our 3D spinal cord induction (3-DiSC) condition recapitulates patterning of the developing dorsal spinal cord and enables the generation of four types of dorsal interneuron marker-positive cell populations. By activating Shh signaling, intermediate and ventral spinal cord-like tissues are successfully induced. After dissociation of these tissues, somatosensory neurons and spinal motor neurons are detected and express neurotransmitters in an *in vivo* manner. Our approach provides a useful experimental tool for the analysis of human spinal cord development and will contribute to research on the formation and organization of the spinal cord, and its application to regenerative medicine.

KEY WORDS: Human pluripotent stem cell, Spinal cord tissue, Development, Spinal interneurons, Spinal motor neurons

INTRODUCTION

Spinal cord tissue consists of well-organized neural circuits that process large amounts of information for the organism to sense its environment and generate motor behavior. During early embryonic development, spinal cord tissues are initially formed from a sheet-like structure termed the neural plate. The neural plate bends towards the dorsal side of the embryo and forms a tubular structure: the neural tube (Novitsch et al., 2003). During dorsal-ventral patterning of the neural tube, more than 20 distinct classes of neurons are generated (Alaynick et al., 2011; Lu et al., 2015). Two organizing centers play important roles in determining the characteristics of neuronal progenitor cells during spinal cord formation. One organizing center is the roof plate (RP), which is located dorsally and induces dorsal progenitor domains by producing bone morphogenetic proteins (BMPs) and Wnts (Timmer et al., 2002;

Chizhikov and Millen, 2004b). The other organizing center is the floor plate (FP), which is located ventrally and induces ventral progenitor domains by producing sonic hedgehog (Shh) (Jessell, 2000). With the help of these two morphogen-producing organizing centers, six discrete dorsal progenitor domains and five ventral progenitor domains are generated along the dorso-ventral axis, and various subclasses of spinal interneurons and motor neurons are generated from the patterned progenitor domains (Goulding, 2009).

Recently, much attention has been paid to the efficient generation of spinal motor neurons from human pluripotent stem cells (hPSCs) (Amoroso et al., 2013; Du et al., 2015; Maury et al., 2015). Several reports describe the induction of patterned neural tube-like structures using mouse embryonic stem cells (ESCs); however, the formation of a three-dimensional (3D) structure of spinal cord tissues that includes the patterned induction of various types of spinal neurons has not been described (Peljto et al., 2010; Meinhardt et al., 2014; Ranga et al., 2016). Because the spinal cord works as an independent functional unit, it is necessary to induce not only single spinal motor neurons, but also total spinal cord tissue if one wants to analyze the spinal cord as a completely functional organ system. The derivation of a 3D spinal cord equivalent would thus allow better understanding of spinal cord development and contribute to the generation of valid *in vitro* disease models.

To overcome the aforementioned limitations, we sought to achieve the 3D induction of spinal cord tissues from hPSCs. By modifying a previously described protocol for spinal motor neurons, we first established a new differentiation condition for dorsal spinal cord-like tissue induction, making it possible to generate four distinct dorsal interneuron marker-positive cell populations. The character of these tissues could be dorsalized by BMP4 treatment. Activation of Shh signaling, on the other hand, led to the successful formation of intermediate and ventral spinal cord-like tissues. Furthermore, these hPSC-derived *in vitro* tissues could generate several types of spinal neurons that mimic patterns of the developing spinal cord *in vivo*. Our hPSC-based *in vitro* induction condition recapitulates the *in vivo* developmental process of spinal cord formation and thus represents a useful tool for studying human spinal cord-related diseases and potentially for drug discovery and regenerative medicine.

RESULTS


Induction of patterned dorsal spinal cord-like tissues from hPSCs

To induce spinal cord tissues, we first induced spinal motor neurons following a previously described protocol (referred to as the SMN protocol). Because our goal was 3D structure formation, we used a SFEBq-based approach, which has previously been shown to efficiently induce 3D neural tissues *in vitro* (Maury et al., 2015; Eiraku et al., 2008). A feeder-free human induced pluripotent cell (iPSC) line (1039A1) was dissociated to single cells and 9000 cells were seeded into each well of U-bottomed 96-well plates with

¹Department of Clinical Application, Center for iPS Cell Research and Application, Kyoto University, 606-8507 Kyoto, Japan. ²Department of Neurosurgery, Kyoto University Graduate School of Medicine, 606-8507 Kyoto, Japan.

*These authors contributed equally to this work

‡Authors for correspondence (hideya.sakaguchi@cira.kyoto-u.ac.jp; jbtaka@cira.kyoto-u.ac.jp)

 H.S., 0000-0001-9628-9360; J.T., 0000-0003-3642-9186

This is an Open Access article distributed under the terms of the Creative Commons Attribution License (<http://creativecommons.org/licenses/by/3.0>), which permits unrestricted use, distribution and reproduction in any medium provided that the original work is properly attributed.

low-adhesion coating. The cells reaggregated quickly to form a single embryoid body per well and were cultured using the SMN protocol (Fig. S1A). On culture day 15, a large number of Olig2⁺/Nkx6.1⁺ spinal motor neuron progenitor cells were identified (Fig. S1B). On day 24, the generation of Hb9⁺/Islet1⁺ motor neuron precursors was confirmed (Fig. S1C). To evaluate the continuous epithelial structure in the aggregates, we examined the expression pattern of N-cadherin. Although PAX6⁺/N-cadherin⁺ neural progenitors were observed in the aggregates on day 15, the expression of N-cadherin was observed only in a discontinuous manner (Fig. S1D-F). This result demonstrated that proper 3D epithelial structure formation could not be obtained under the SMN condition.

To form the 3D structure of spinal cord tissues, we tried to establish a new condition. Many small molecules were included in the original SMN protocol to modulate signaling pathways and restrict the generated cell populations to spinal motor neurons. We hypothesized that eliminating some of the small molecules would induce wider regions of the spinal cord. We tested the modified condition under which LDN193189 (BMP inhibitor) and SAG (smoothed agonist) were removed with supplementation of basic differentiation medium [referred to as the 3-dimensional spinal cord (3-DiSC) condition] (Fig. 1A). Under this condition, continuous epithelial structures were observed in the aggregates on day 15 (Fig. 1B,C). Immunohistochemistry (IHC) analysis showed the efficient formation of PAX6⁺/N-cadherin⁺ continuous neuroepithelial structures (Fig. 1D-F).

Next, we examined the character of the progenitors in the formed continuous neuroepithelium. Because each progenitor domain can be distinguished by the expression pattern of distinct transcription factors, we first checked the expression of progenitor domain markers using quantitative PCR (qPCR) (Fig. 1G) (Lu et al., 2015). Under the SMN protocol, the expression of Olig2 (marker for pMN) was evident, while the expression of markers for dorsal domains such as Lmx1a (a marker for roof plate), Olig3 [a marker for progenitor domains 1-3 (pd1-3)] and PAX7 (a marker for dorsal progenitor domains) was not (Fig. 1H). Conversely, under the 3-DiSC condition, the expression of Olig2 was repressed, while the expression of the aforementioned dorsal domain markers was strongly upregulated.

We further analyzed and validated the properties of hPSC-derived 3D continuous epithelial structures by IHC. Continuous epithelial structures mainly expressed PAX6 and PAX7, suggesting the generation of dorsal progenitor domains (Fig. 1I,L). Several regions in the Pax6⁺ neuroepithelium showed the expression of Olig3 (Fig. 1J,M). Adjacent to the Pax6⁺ Olig3⁺ regions, the expression of Lmx1a could be observed, suggesting the generation of Lmx1a⁺ roof plate next to Olig3⁺ pd1-3 domains (Fig. 1K,N). The expression pattern of these markers was similar to the developing embryonic dorsal spinal cord (Fig. 1O). The formation of the structures was observed in 93.4% of the analyzed aggregates in four independent experiments. We obtained similar results for other human iPSC lines and a human ESC line (Fig. S2A-P).

Taken together, our 3-DiSC condition enabled the efficient *in vitro* induction of continuous epithelial structures that express several dorsal progenitor domain markers, which is similar to the developing embryonic dorsal spinal cord.

Neural fate commitment in early phase under 3-DiSC condition and the emergence of roof plate-like structures

Next, we examined how patterned dorsal progenitor domains were formed from hPSC aggregates. We first investigated the morphological change and neural marker expression pattern of

the aggregates. After hPSCs were seeded into each well of a U-bottomed 96-well plate, a cell aggregate became obvious from 10 h after the start of differentiation (Movie 1). Imaging also showed that a small number of cells surrounded and were not integrated into the aggregate. On day 3, round-shape aggregates were formed (Fig. 2A); on day 6, a continuous epithelial structure was obviously generated; and on day 9, several small protrusions were formed in the aggregates (Fig. 2A',A''). The expression of SOX1/SOX2 was broadly seen in the aggregates at day 3, but it was restricted to the neuroepithelial structure on day 6 (Fig. 2B,B',C,C'). The expression of PAX6 was also observed in the epithelium after day 6 (Fig. 2D,D'). The expression of SOX1/SOX2/PAX6 became more apparent in the epithelial structure at day 9 (Fig. 2B'',C'',D''). By contrast, under SMN protocol condition, no continuous epithelial structure was formed from days 3 to 9. Instead a SOX2⁺/PAX6⁺ rosette-like structure was formed in the aggregates (Fig. S1G-H''). The continuous epithelium under 3-DiSC condition widely expressed N-cadherin on day 9, and the expression pattern was dense in the outer side of the epithelium (Fig. 2G). The expression of apical marker aPKC was also observed mainly in the same area, indicating the continuous epithelial structure formed an apical surface on its outside from the early stage of differentiation (Fig. 2G'). On day 9, the expression of Lmx1a was observed on the small protrusions (Fig. 2H). These observations confirmed the generation of a neuroepithelium structure up to day 6 and the emergence of Lmx1a⁺ roof plate-like small protrusions at day 9 under the 3-DiSC condition.

Because BMP inhibitors, which are known to promote neural differentiation, were removed under the 3-DiSC condition, we also evaluated other lineage cells. Regarding neural crest lineage, a small number of SOX10⁺ cells were generated, but they were confined to the inner part of the aggregates (Fig. 2E-E''). Concerning mesodermal lineage, brachyury⁺ cells could not be detected after day 3 (Fig. 2F-F''). These data suggested our 3-DiSC condition mainly induced neural lineage from the early stage of differentiation.

In the developing embryonic dorsal spinal cord, roof plate plays an important role as a dorsal organizing center that produces BMPs and Wnts, which are responsible for the patterning of the dorsal spinal cord (Chizhikov and Millen, 2004b; Lee et al., 2000). We speculated the involvement of roof plate-like morphogen-generating structures in the generation of the patterned dorsal spinal cord tissue under our 3-DiSC condition, and assessed the expression pattern of BMP and Wnt signaling-related markers around the roof-plate-like protrusions. On day 9, MSX1 and MSX2, both of which are downstream targets of BMPs, were expressed in a region beyond the Lmx1⁺ region (Fig. 2H'). Other downstream targets of BMPs, such as phospho-Smad 1/5, were also observed in the protrusion (Fig. 2I,I'), and the expression of Wnt1 was detected around the Lmx1a⁺ regions (Fig. 2J,J'). These observations are consistent with the idea that Lmx1a⁺ protrusions play a role as an organizing center by producing inductive signals such as BMP and Wnt (Fig. 2K). Based on the above, we concluded that our 3-DiSC condition could efficiently induce continuous neuroepithelium for the first 6-9 days with self-forming roof plate-like protrusions, which have the potential to produce inductive signals.

BMP4 treatment dorsalized the identity of spinal cord-like tissues

Next, we tried to further dorsalize the induced spinal cord-like tissues. In the developing spinal cord, dorsal interneurons (dIs) are generated toward the outside of the progenitor zone. Dorsal interneurons are

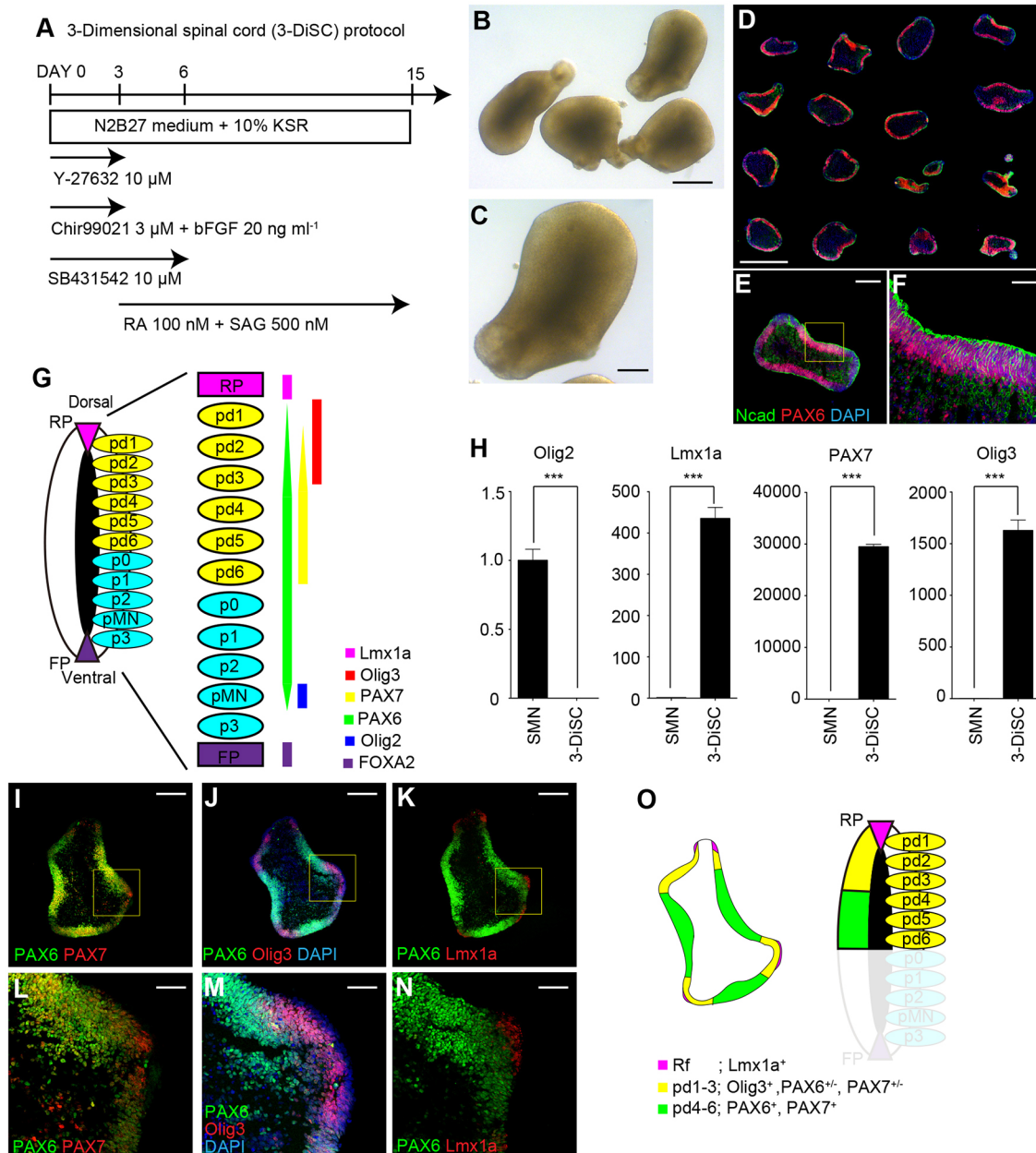


Fig. 1. Induction of patterned dorsal spinal cord-like tissues from hPSCs. (A) Schematic of the differentiation protocol for spinal cord tissues (the 3-DiSC condition). (B,C) Phase-contrast images of the aggregates on day 15. (D-F) A PAX6⁺/N-cadherin⁺ continuous neuroepithelial structure was efficiently formed on day 15. (G) Schematic showing the expression pattern of progenitor domain markers in the developing spinal cord. (H) qPCR analysis on day 15 showing the relative expression of progenitor domain markers under the 3-DiSC condition compared with the SMN condition (***) $P < 0.001$, $n = 6$ total RNA samples from three independent culture experiments, unpaired t -test with Welch's correction, two-tailed). Data are mean \pm s.e.m. (I-K) Immunostaining of serial section of an aggregate on day 15 showed the generation of dorsal spinal cord-like tissues. (I,L) The PAX6⁺ continuous epithelium co-expressed PAX7. (J,M,K,N) Several regions in the Pax6⁺ neuroepithelium showed the expression of Olig3, and Lmx1a⁺ domains were induced adjacent to Pax6⁺/Olig3⁺ domains. (O) Schematic summary showing the dorsal spinal cord-like tissues induced by the 3-DiSC condition. Scale bars: 1000 μ m in D; 500 μ m in B; 200 μ m in C,E,I-K; 50 μ m in F,L-N.

divided into six discrete subclasses (dl1-6) and can be distinguished by the combination of expressed transcription factors (Fig. 3B, Fig. S3A-F) (Müller et al., 2002; Gross et al., 2002). As BMP4 is required for the generation of the dorsal-most subclass, we compared BMP4-treated conditions and non-treated conditions (Fig. 3A) (Le Dreau et al., 2012). We first examined the expression of dorsal interneuron markers using qPCR. Compared with non-treated conditions, the expression of Lbx1 (a marker for dl4-6) was significantly repressed upon BMP4 treatment, whereas the expression of Brn3a (a marker for dl1-3 and dl5) was upregulated (Fig. 3C).

These results suggested that BMP4 treatment dorsalized the character of the generated interneurons.

Next, we focused in more detail on the detection and characterization of each dorsal interneuron population by IHC. Under non-treated conditions, both Brn3a⁺ and PAX2⁺ populations were observed in different regions (Fig. 3D). In the Brn3a⁺ population cells, Lhx9⁺, Lhx1⁺ and Islet1⁺ cells were identified, suggesting them to be dl1, dl2 and dl3, respectively (Fig. 3E,G-I). PAX2⁺ cells co-expressed Lhx1, suggesting that they were dl4 or dl6 (Fig. 3F,J). These findings indicated that four

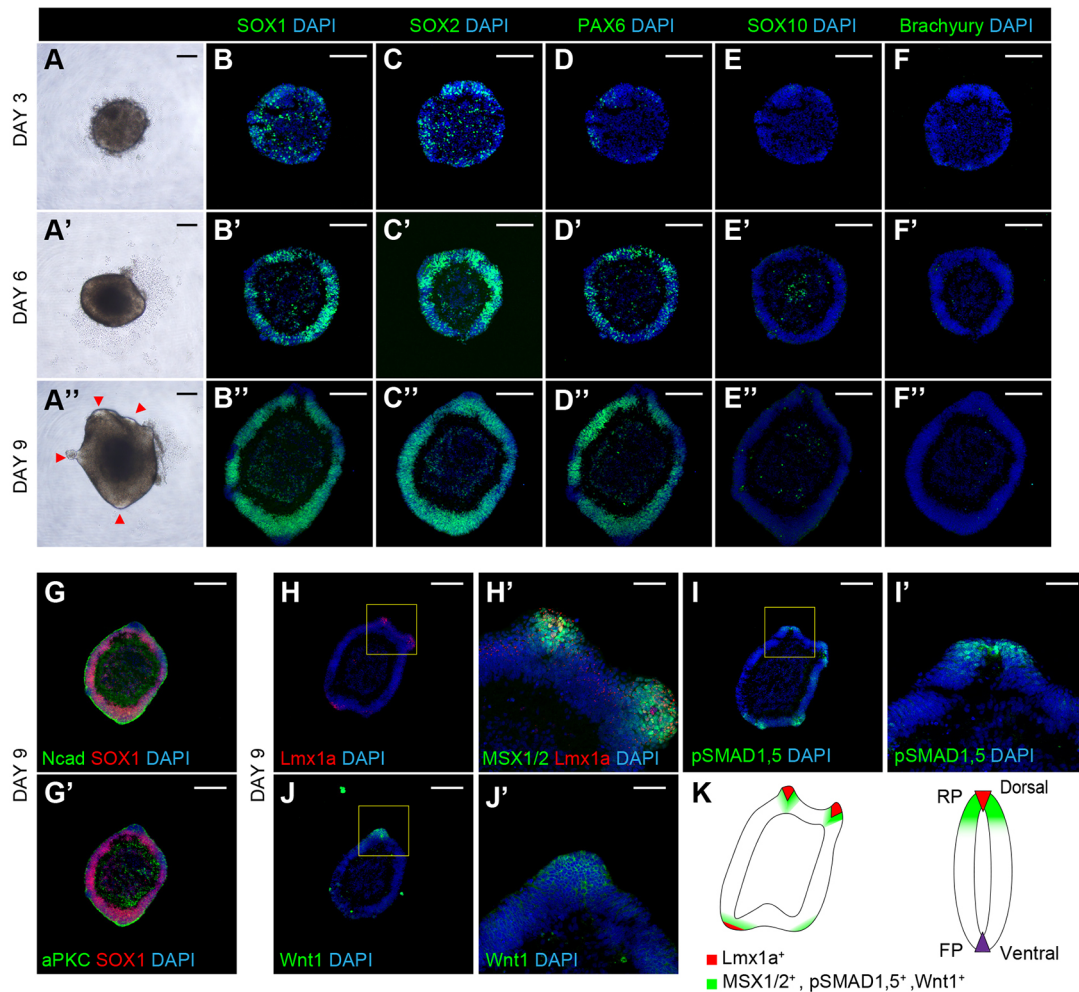


Fig. 2. Neural fate commitment in early phase under the 3-DiSC condition and the emergence of roof plate-like structures. (A-A'') Phase-contrast images during the early phase of the culture period showing the generation of the continuous epithelial structure and several protrusions. Small protrusions were formed on the epithelial structure from day 9 (red arrowheads in A''). (B-F'') Immunostaining of aggregates cultured under the 3-DiSC condition for SOX1, SOX2, PAX6, SOX10 and brachyury. (B-B'', C-C'', D-D'') A SOX1⁺ SOX2⁺ PAX6⁺ continuous neuroepithelial structure was formed for the first 6-9 days. (E-E'') A small number of SOX10⁺ cells were observed, and the cells were confined to the inner part of the aggregate. (F-F'') Brachyury⁺ cells were rarely detected. (G, G') N-cadherin and aPKC were mainly expressed in the outer side of the epithelium. (H, H') Immunostaining for Lmx1a and MSX1/2. (H) The expression of Lmx1a was observed on the protrusion. (H') MSX1/2 was expressed in a wider region than the Lmx1a⁺ region. (I, I') Immunostaining for phospho-Smad 1/5. The expression of phospho-Smad 1/5 correlated with the expression of MSX1/2. (J, J') Immunostaining for Wnt1. The expression of Wnt1 was also detected around the protrusion structure. (K) Schematic summary showing the expression pattern of BMP and Wnt signaling-related markers. Scale bars: 200 μ m in A-H, I, J; 50 μ m in H', I', J'.

types of dorsal interneuron marker-positive cells were detected under non-treated conditions. Under BMP4-treated conditions, the proportion of PAX2⁺ cells was remarkably decreased, whereas the Brn3a⁺ population increased (Fig. 3K). Among Brn3a⁺ cells, Lhx9⁺ and Lhx1⁺ cells were distributed separately (Fig. 3L, N, O). Only a few Brn3a⁺/Islet1⁺ cells and PAX2⁺/Lhx1⁺ cells were detected (Fig. 3M, P, Q). Compared with non-treated conditions, the percentage of the dI1 marker-positive cell population was significantly increased, that of dI2 was unchanged, and those of dI3 and dI4 were significantly decreased (Fig. 3R). This BMP treatment did not affect SOX2 expression and did not promote SOX10⁺ neural crest cell generation (Fig. S4A, B). To investigate whether other BMP subtypes could dorsalize the induced spinal cord-like tissues, we tested BMP7 treatment. Under BMP7-treated conditions, dI4/6 marker-positive (Lhx1⁺/PAX2⁺) cells were decreased and dI1 marker-positive (Brn3a⁺/Lhx9⁺) cells were increased compared with the non-treated condition, indicating BMP7

treatment could also dorsalize the tissues (Fig. S4C-C'', D-D''). These results indicate that BMP treatment dorsalized the induced spinal cord-like tissues, mainly giving rise to dI1 and dI2 marker-positive cells.

Next, we examined the interplay between retinoic acid (RA) and BMPs. As RA activates the expression of PAX6, while BMP signaling represses the expression of PAX6 and induces dorsal-most progenitor domains (Novitsch et al., 2003; Timmer et al., 2002), we hypothesized that the elimination of RA would enhance the effect of BMP signaling and dorsalize the generated cellular character. We tested the effect of RA removal between days 15 and 24 on the two BMP4 groups. Concerning the non-treated group, RA removal decreased dI4/6 marker-positive (PAX2⁺/Lhx1⁺) cells, but increased dI1 marker-positive (Brn3a⁺/Lhx9⁺) cells (Fig. S5A-A'', B-B''). Concerning the BMP4-treated group, RA removal increased dI1 marker-positive (Brn3a⁺/Lhx9⁺) cells, but decreased dI2 marker-positive (Brn3a⁺/PAX2⁺) cells (Fig. S5C-C'', D-D''). These data

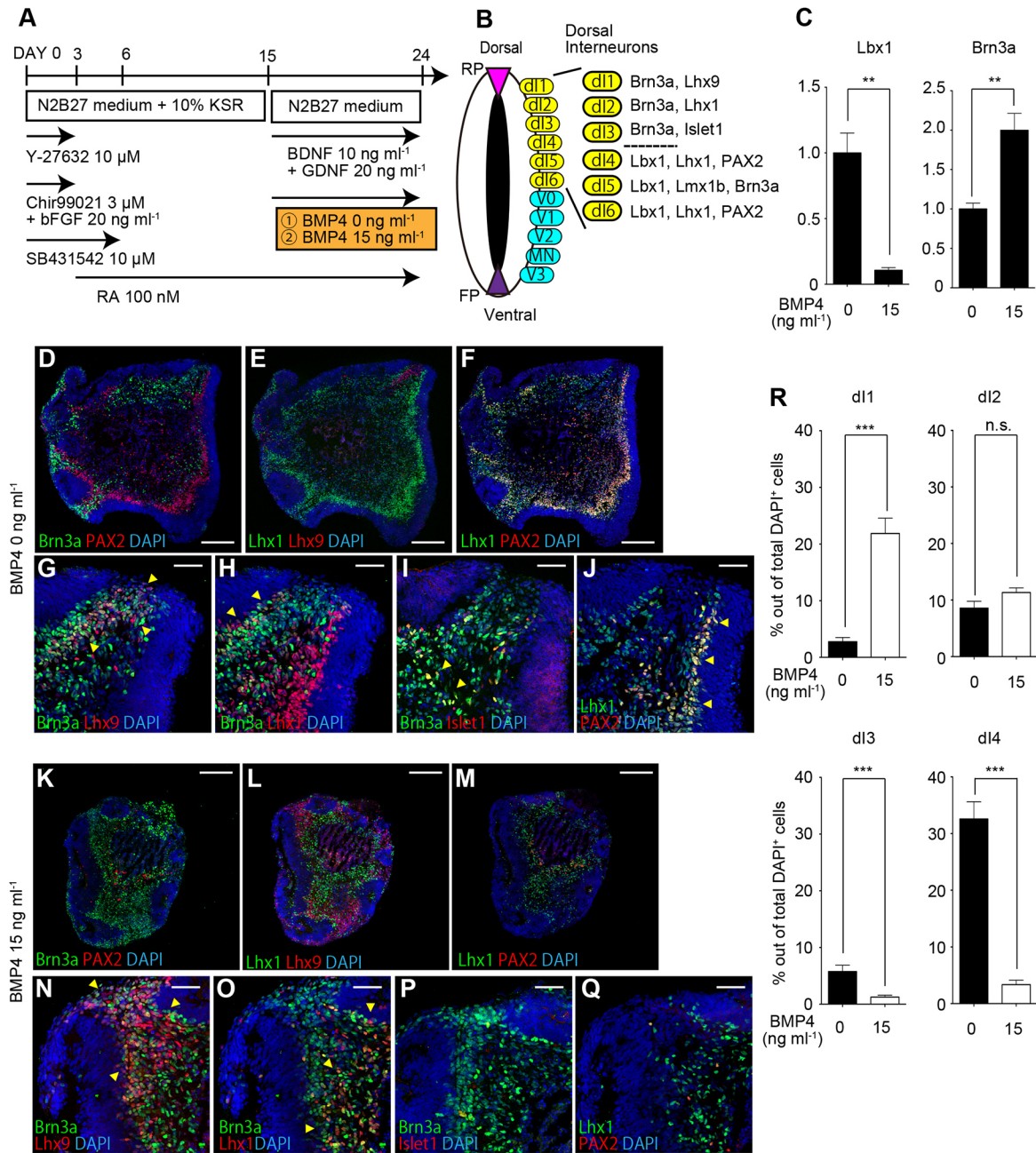


Fig. 3. BMP4 treatment dorsalized the identity of spinal cord-like tissues. (A) Schematic of the examined conditions. (B) Schematic showing the marker expression of each dorsal interneuron subclass. (C) qPCR analysis on day 24 showing the relative expression of dorsal interneuron markers under BMP4-treated condition compared with non-treated condition (** $P < 0.01$, $n = 7$ total RNA samples from three independent culture experiments, unpaired t -test with Welch's correction, two-tailed). Data are mean \pm s.e.m. (D–J) Immunostaining under BMP 0 ng ml^{-1} condition on day 24. (D) Brn3a⁺ and PAX2⁺ populations exhibited separate distributions. (E) An Lhx9⁺ population was observed on the tip of the aggregates. (F) The PAX2⁺ population co-expressed Lhx1. (G–J) Lhx9⁺/Brn3a⁺, Lhx1⁺/Brn3a⁺, Islet1⁺/Brn3a⁺ and PAX2⁺/Lhx1⁺ populations were suggested to be dl1, dl2, dl3, and dl4 or dl6, respectively. (K–Q) Immunostaining under BMP 15 ng ml^{-1} condition on day 24. (K) A Brn3a⁺ population was mainly generated. (L) Lhx9⁺ and Lhx1⁺ populations exhibited separate distributions. (M) PAX2⁺/Lhx1⁺ cells were rarely observed. (N, O) Lhx9⁺/Brn3a⁺ (dl1) and Lhx1⁺/Brn3a⁺ (dl2) populations were mainly generated. (P, Q) Islet1⁺/Brn3a⁺ (dl3) and PAX2⁺/Lhx1⁺ (dl4 or dl6) populations were rarely observed. (R) Percentages of each population among total DAPI⁺ cells. Data are mean \pm s.e.m. (***) $P < 0.001$, n.s., not significant; $n = 9$ aggregates from three independent experiments). Scale bars: 200 μm in D–F, K–M; 50 μm in G–J, N–Q.

suggest that the removal of RA also leads to the dorsalization of generated cellular character (Fig. S5E). Collectively, these results demonstrate that our 3-DiSC condition can induce spinal cord-like tissue with four different types of dorsal interneurons, and that the cellular character of the generated cell populations can be changed and dorsalized by BMP4 treatment or RA removal.

Spinal cord-like tissues were ventralized by activating Shh signaling in a dose-dependent manner

Next, we tried to ventralize the hPSC-derived spinal cord-like tissues. Because a Shh gradient contributes to the patterning of ventral progenitor domains in the developing spinal cord, we examined the effect of SAG treatment on *in vitro*-derived 3D human

spinal cord-like tissues to mimic the activation and presence of Shh signaling (Fig. 4A) (Ribes and Briscoe, 2009). We tested three conditions: SAG 0 nM (control), SAG 50 nM (moderate) and SAG 500 nM (strong). We initially assessed the gene expression of progenitor domain markers using qPCR (Fig. 4B) (Lu et al., 2015). Under SAG 50 nM and SAG 500 nM, the dorsal domain markers *Lmx1a*, *Olig3* and *PAX7* were downregulated (Fig. 4C). Regarding intermediate domain markers, the expression of *Dbx1* and *Dbx2* was significantly increased under SAG 50 nM, but not under SAG 500 nM (Fig. 4D). On the other hand, the expression of ventral domain markers such as *Nkx6.1*, *Olig2* and *FOXA2* was unperturbed by SAG 50 nM, but increased significantly under SAG 500 nM (Fig. 4E). These results suggested that SAG treatment could ventralize the progenitor domain identity in a dose-dependent manner.

To evaluate the structure, we further analyzed the expression patterns of progenitor domain markers in the aggregates by IHC. Continuous epithelial structures were formed under all conditions (Fig. S6A,E,I). Under SAG 0 nM, the expression of both *PAX6* and *PAX7* was observed in the continuous epithelium, but no expression of intermediate or ventral progenitor markers, such as *Dbx1*, *Dbx2*, *Olig2* or *Nkx2.2*, was observed, which confirmed the generation of dorsal progenitor domains (Fig. 4F–J, Fig. S6A–D).

Under SAG 50 nM, *PAX7* was not expressed, but *PAX6* expression was maintained, suggesting the induction of ventral progenitor domains (Fig. 4K, Fig. S6E–H). In the *PAX6*⁺ continuous epithelium, *Dbx1*⁺ and *Nkx6.1*⁺ cells were observed to cover distinct regions within the epithelium (Fig. 4L,M). *Dbx1*⁺ regions were suggested to be the p0 domain. In the *Nkx6.1*⁺ regions, the expression of *Olig2* was scarcely observed, suggesting *Nkx6.1*⁺ regions to correspond to the p2 domain (Fig. 4N). Furthermore, the p0 domain (*Dbx1*⁺) and p2 domain (*Nkx6.1*⁺/*Olig2*[−]) regions were not adjoined (Fig. 4O). *Evx1*⁺ (marker for V0) cells and *Chx10*⁺ (marker for V2a) cells were generated on day 24 (Fig. S6O,P). Together, these findings suggested the formation of an intermediate (ventral-dorsal) spinal cord-like structure under SAG 50 nM.

Under SAG 500 nM, the expression of *PAX7* was again absent, but the expression of *PAX6* was partially maintained (Fig. 4P, Fig. S6L,J). In the continuous epithelium, *Olig2*⁺ regions and *Nkx2.2*⁺ regions could be identified, suggesting the generation of the pMN domain and p3 domain, respectively (Fig. 4Q). *Nkx6.1* was expressed widely in the same areas as *Olig2*⁺ (marker for pMN) and *Nkx2.2*⁺ regions (marker for p3), which is consistent with the expression patterns observed *in vivo* (Fig. 4R,S). The expression of *FOXA2* (a marker for floor plate) was also observed in the aggregates (Fig. 4T, Fig. S6K,L). Some *FOXA2*⁺ cells co-expressed *Arx*, suggesting the generation of definitive floor plate (Fig. S6M) (Cho et al., 2014; Mansour et al., 2014). Notably, pMN (*Olig2*⁺), p3 (*Nkx2.2*⁺) and FP (*FOXA2*⁺) domains were aligned in a manner similar to the pattern observed during development of the ventral spinal cord *in vivo* (Fig. 4T) (Ribes et al., 2010). *Hb9*⁺, *Islet1*⁺ and *Hb9*⁺*Islet1*⁺ cells were generated on day 24, and some co-expressed *Foxp1*, suggesting the generation of spinal motor neurons, including lateral column type (Fig. S6Q–S). These findings suggested the formation of ventral spinal cord-like structures under SAG 500 nM. To summarize, these results demonstrated that SAG treatment ventralized the progenitor domain identity in a dose-dependent manner, making it possible to induce several distinct domains within a continuous neuroepithelial structure and to recapitulate the patterning of the developing intermediate and ventral spinal cord.

Furthermore, we evaluated the positional identity of the aggregates along their rostral-caudal (R–C) axis under SAG

500 nM. The positional identities are determined by the expression patterns of genes in the HOX loci (Fig. S7A) (Philippidou and Dasen, 2013). On day 15, qPCR analysis clearly detected the expression of *HOXC5* and *HOXC6* but not of *HOXC8*, *HOXC9* or *HOXC10*, suggesting the induced ventral spinal cord tissues corresponded to rostral cervical level spinal cord (Fig. S7C). Because FGFs play key roles in inducing and regulating progressive HOX activation, we tested the effect of prolonged FGF treatment (6 days; long-FGF condition) and compared the expression pattern of HOX genes with the control condition (Fig. S7B) (Mazzoni et al., 2013; Lippmann et al., 2015). Under the long-FGF condition, the expression of *HOXC5* was not significantly changed, but the expression of *HOXC9* was upregulated strongly (Fig. S7D). The expression of *HOXC10* was still not evident. These results suggested the induction of thoracic levels under long-FGF. To summarize, rostral cervical level was induced under SAG 500 nM and the positional identity could be caudalized up to the thoracic level by prolonging FGF treatment.

Generation of two distinct V2 interneuron subtypes

In the developing ventral spinal cord, the p2 domain yields several types of interneurons. Among them, the balance of excitatory V2a interneurons and inhibitory V2b interneurons is controlled by Notch signaling (Fig. 5A) (Joshi et al., 2009). The proportion of V2a interneurons is increased upon Notch inhibition. On the other hand, the specification of V2b interneurons requires Notch signaling. Because we identified p2 domains in the aggregates under SAG 50 nM, we examined the spinal cord-like 3D tissues on day 24 for the expression of V2a and V2b interneuron markers under the SAG 50 nM condition. IHC showed that the majority of cells expressed *Lhx1* and *PAX2*, suggesting the presence of V0 or V1 interneurons (Fig. 5C). In addition, both *Chx10*⁺ (V2a interneuron marker) cells and *GATA3*⁺ (V2b interneuron marker) cells were observed in the analyzed 3D structures (Fig. 5D–F). These observations indicated that V0, V1, V2a and V2b marker-positive cells could be detected in 3D structures cultured under SAG 50 nM. In order to assess the effect of Notch signaling, we tested DAPT (Notch inhibitor) treatment and evaluated the composition of the V2 population (Fig. 5B). IHC showed a substantial number of *Chx10*⁺ cells, whereas *GATA3*⁺ cells were scarcely detected (Fig. 5G–J). Inhibition of Notch signaling increased the percentage of the *Chx10*⁺ population among total V2 interneuron marker-positive cells from 72.1% to 98.7% (Fig. 5K). These findings indicate that the division of V2a and V2b populations via Notch signaling could be recapitulated via our *in vitro* 3D induction system.

Dissociated neurons show same expression patterns as somatosensory neurons and spinal motor neurons

Last, we examined whether hPSC-derived dorsal or ventral spinal cord-like tissues could generate subtypes of spinal interneurons or spinal motor neurons. Each subclass of spinal neurons expresses a defined set of neurotransmitters (Fig. 6A) (Lu et al., 2015). Cholinergic spinal motor neurons express choline acetyltransferase (*CHAT*); dI1-3-derived somatosensory relay neurons and V2a interneurons are glutamatergic neurons that express *Vglut2*; and dI4-derived somatosensory associative neurons and dI6 interneurons are GABAergic neurons that express *GAD67*.

Because it is difficult to evaluate the character of a single neuron in 3D aggregates, we performed dissociation cultures, which enabled us to evaluate the presence of distinct neurotransmitters. The spinal cord-like aggregates generated under the different SAG conditions were dissociated around day 40 and plated on

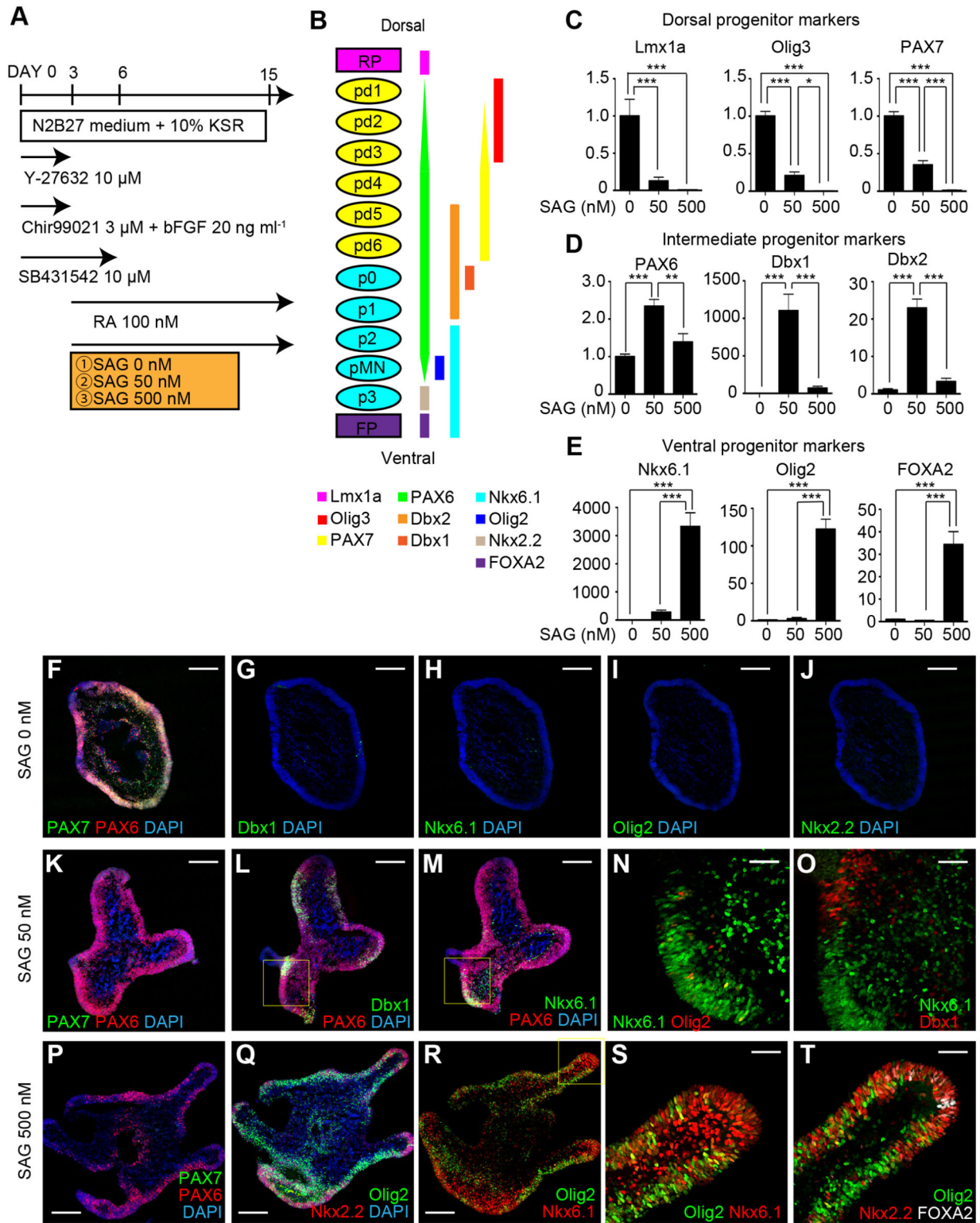


Fig. 4. Spinal cord-like tissues were ventralized by activating Shh signaling in a dose-dependent manner. (A) Schematic of the examined conditions. (B) Schematic showing the expression pattern of progenitor domain markers in the developing spinal cord. (C-E) qPCR analysis on day 15 showing the relative expression of dorsal progenitor markers (C), intermediate progenitor markers (D) and ventral progenitor markers (E). Fold changes compared with SAG 0 nM ($*P < 0.05$, $**P < 0.01$, $***P < 0.001$, $n = 7$ total RNA samples from three independent culture experiments, one-way analysis of variance followed by post-hoc Tukey's test). Data are mean \pm s.e.m. (F-J) Immunostaining under SAG 0 nM on day 15. PAX7 was widely expressed, whereas no ventral markers such as Dbx1 (G), Nkx6.1 (H), Olig2 (I) or Nkx2.2 (J) were detected. (K-O) Immunostaining under SAG 50 nM. (K) The continuous epithelium expressed PAX6 but not PAX7. (L,M) Dbx1⁺ and Nkx6.1⁺ domains were induced. (N) Olig2 was scarcely expressed in Nkx6.1⁺ domains. (O) Dbx1⁺ and Nkx6.1⁺ domains did not adjoin each other. (P-T) Immunostaining under SAG 500 nM. (P) The continuous epithelium partially expressed PAX6 but not PAX7. (Q) Olig2⁺ and Nkx2.2⁺ domains were mainly induced. (R,S) Nkx6.1 was widely expressed. (T) FOXA2⁺, Nkx2.2⁺ and Olig2⁺ domains aligned similarly to how they aligned in *in vivo* developing ventral spinal cord. Scale bars: 200 μ m in F-M,P,R; 50 μ m in N,O,S,T.

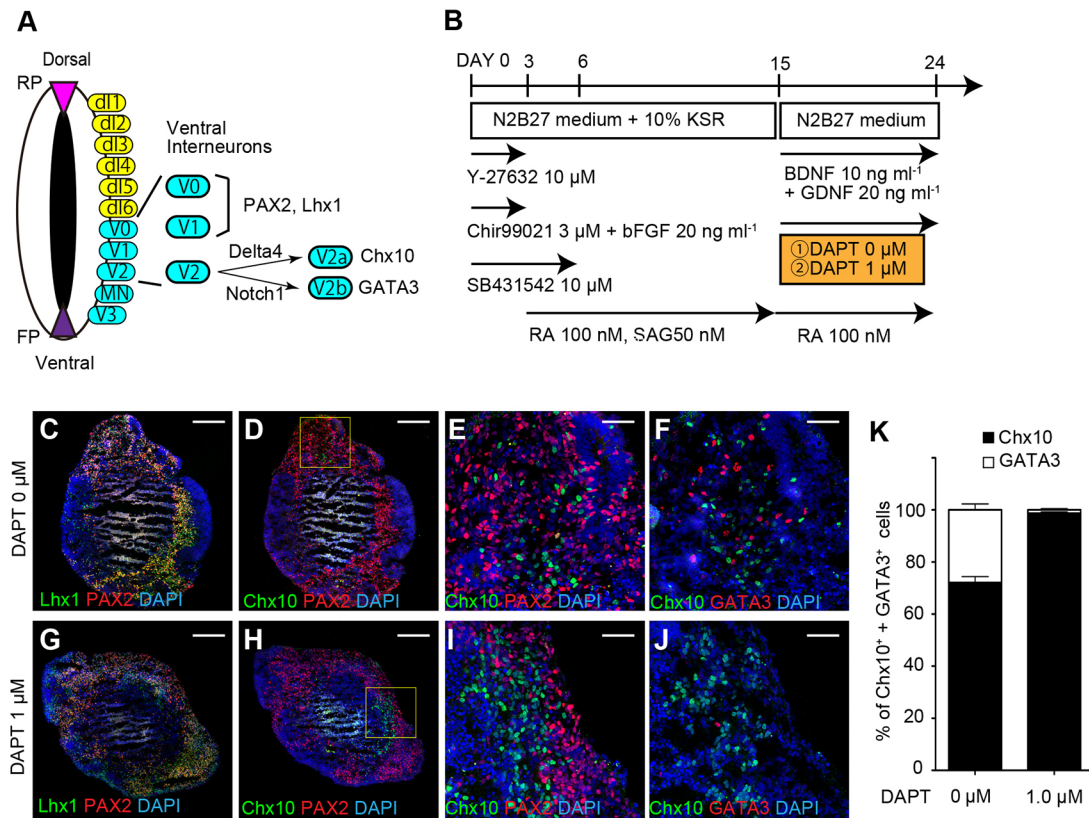


Fig. 5. Generation of two distinct V2a interneuron subclasses. (A) Schematic showing the marker expression of V0-2 interneurons. (B) Schematic of the examined conditions. (C-F) Immunostaining under DAPT 0 μM on day 24. (C) An Lhx1⁺/PAX2⁺ population was suggested to be V0 or V1. (D-F) Both Chx10⁺ (V2a marker) cells and GATA3⁺ (V2b marker) cells were detected. (G-J) Immunostaining under DAPT 1 μM . Although Chx10⁺ (V2a marker) cells were observed, only a few GATA3⁺ (V2b marker) cells were detected. (K) Percentages of each population ($n=9$ aggregates from three independent experiments). Data are mean \pm s.e.m. Scale bars: 200 μm in C,D,G,H; 50 μm in E,F,I,J.

poly-D-lysine-laminin-fibronectin-coated plates (Fig. 6B). After dissociation, the plated cells started to elongate axons and form networks (Fig. 6C). On day 18 after the dissociation, flattened glial shaped cells also emerged (Fig. 6C, day 18).

Under all conditions, IHC confirmed the generation of a Tuj1⁺ neuronal population and a GFAP⁺ glial population (Fig. 6D,E,M,N,R,S). Under SAG 0 nM, among Tuj1⁺ neurons, the primary populations were Vglut2⁺ neurons and GABA⁺ neurons (Fig. 6F,G,L,J). Vglut2⁺ neurons expressed Bm3a or Islet1, suggesting that they were somatosensory relay neurons derived from dI1-3 (Fig. 6H). GAD67⁺ and GABA⁺ neurons expressed PAX2, suggesting they were dI4-derived somatosensory associative neurons or dI6 interneurons (Fig. 6K,L). Under SAG 50 nM, IHC also showed Vglut2⁺ neurons expressing Chx10, calbindin⁺ neurons expressing MafB and GABA⁺ neurons expressing Foxp2, suggesting that they were glutamatergic V2a interneurons, Renshaw interneurons and non-Renshaw V1 interneurons, respectively (Fig. 6O-Q) (Stam et al., 2012). Under SAG 500 nM, the main population consisted of ChAT⁺ neurons (Fig. 6T). These neurons expressed Islet1 or Hb9, or both, suggesting the generation of spinal motor neurons (Fig. 6U,V). To summarize, spinal cord-like tissues induced from hPSCs under defined conditions enabled the *in vitro* generation of several types of human spinal neurons, including somatosensory relay neurons, somatosensory associative neurons and spinal motor neurons.

DISCUSSION

In this report, we demonstrated the 3D induction of spinal cord-like tissues from human PSCs. By modifying a previously described

protocol for *in vitro* spinal motor neuron induction (SMN protocol), we successfully induced dorsal spinal cord-like tissues and generated four types of dorsal interneuron marker-positive cell populations. The character of these tissues could be dorsalized by BMP4 treatment. On the other hand, activation of Shh signaling led to the derivation of intermediate and ventral spinal cord-like tissues in a dose-dependent manner. These *in vitro*-derived spinal cord-like tissues were confirmed to give rise to several subclasses of spinal neurons (Fig. S8).

Most notably, our method enabled the simultaneous induction of several domains and maintained the induced patterns in a 3D structure. By omitting several factors, which usually restrict the direction of differentiation, we could induce a wider region of the dorsal spinal cord, including the Lmx1a⁺ roof plate region. Furthermore, these dorsal spinal cord-like tissues could generate four types of dorsal interneurons, which each exhibited distinct distribution patterns. Although some previous reports have demonstrated the generation of dorsal interneurons, none has provided a detailed evaluation of the neuronal subclasses in 3D structure (Meinhardt et al., 2014; Maury et al., 2015; Gupta et al., 2018). In contrast, our culture condition enabled the stepwise efficient induction of dorsal interneurons and their respective subclasses from hPSCs in 3D. Our 3-DiSC condition is expected to increase understanding of the development of the human somatosensory system, which is mainly organized by dorsal interneurons.

Besides the generation of several subclasses of spinal neurons, the 3D induction of spinal cord tissues enabled the simultaneous

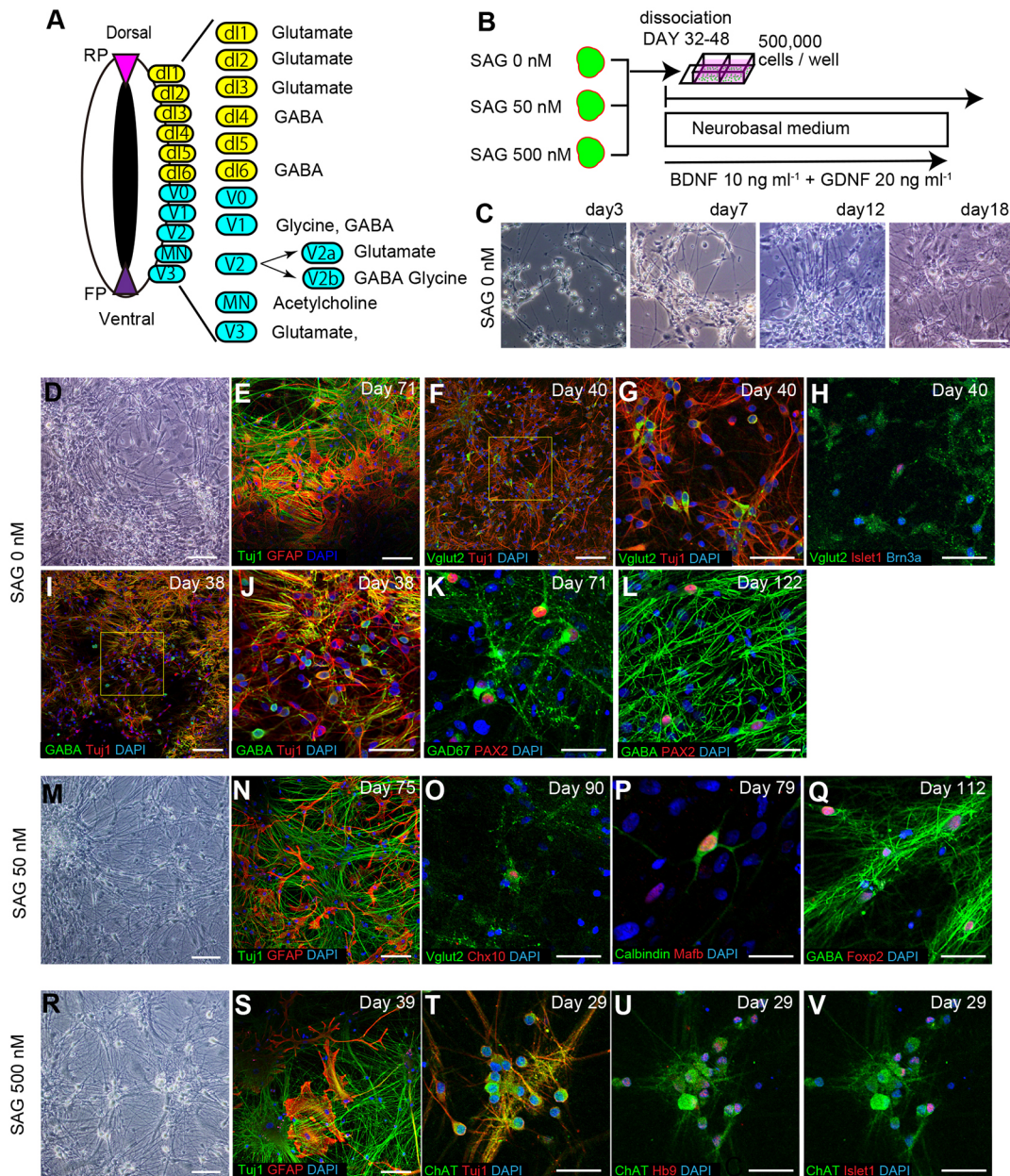


Fig. 6. Dissociated neurons showed expression patterns of somatosensory neurons and spinal motor neurons. (A) Schematic showing the expression pattern of neurotransmitters. (B) Schematic of the protocol for dissociation culture. (C) Phase-contrast images in the early days after dissociation showing neurite extension and the emergence of flat-shaped cells. (D) Phase-contrast image under SAG 0 nM. (E) Immunostaining revealed the presence of both Tuj1⁺ neurons and GFAP⁺ glial cells. (F,G) Vglut2⁺/Tuj1⁺ glutamatergic neurons were detected. (H) Vglut2⁺ neurons expressing Brn3a or Islet1 were suggested to be somatosensory relay neurons derived from dl1-3. (I,J) GABA⁺/Tuj1⁺ neurons were detected. (K,L) GAD67⁺ and GABA⁺ neurons expressing PAX2 were suggested to be dl4-derived somatosensory associative neurons or dl6 interneurons. (M) Phase-contrast image under SAG 50 nM. (N) Both Tuj1⁺ neurons and GFAP⁺ glial cells were generated. (O) Vglut2⁺/Chx10⁺ neurons were suggested to be V2a interneurons. (P,Q) Calbindin⁺/MafB⁺ neurons and GABA⁺/Foxp2⁺ neurons were suggested to be V1 Renshaw interneurons and non-Renshaw V1 interneurons, respectively. (R) Phase-contrast image under SAG 500 nM. (S) Both Tuj1⁺ neurons and GFAP⁺ glial cells were generated. (T) ChAT⁺/Tuj1⁺ cholinergic neurons were detected. (U,V) ChAT⁺ neurons expressed Islet1 or Hb9, or both, suggesting the generation of spinal motor neurons. Scale bars: 100 μm in C-F,I,M,N,R,S; 50 μm in G,H,J-L,O,Q,T-V; 25 μm in P.

generation of roof plate-like organizing centers along with the neuroepithelium. The generation of the roof plate-like structure might be a key factor for the patterned formation of dorsal progenitor domains. We suggest a possible mechanism as follows. First, a small region of the epithelial structure begins to express Lmx1a. The Lmx1a⁺ domains then go on to express inductive factors, including BMPs and Wnts, allowing them to function as a dorsalizing organizing center. Finally, these inductive factors affected the surrounding neuroepithelium, making it possible to

induce several dorsal domains with pattern formation, which is consistent with *in vivo* tissue. Previous *in vivo* studies have shown that Lmx1a is sufficient for roof plate induction and several components of roof plate signaling, including BMP4, GDF7 and Wnt1 (Chizhikov and Millen, 2004a). These signals are all essential for dorsal spinal cord patterning, but their roles depend on the factors and their downstream targets, such as MSX1-3 (Duval et al., 2014; Chizhikov and Millen, 2005; Liu et al., 2004). A future investigation of hPSC-derived spinal cord induction should focus on the mechanistic

analysis, especially with regards to the factors that determine the self-organization of patterned spinal cord neuroepithelium.

Our 3-DiSC condition is also applicable to the induction of ventral spinal cord, including ventral interneurons. Because V0-V3 interneurons constitute the core elements of the local locomotor circuitry, they have been studied from a variety of viewpoints (Goulding, 2009; Benito-Gonzalez and Alvarez, 2012; Borowska et al., 2013; Bikoff et al., 2016). Some recent studies have described the efficient generation of V2a interneurons from mouse and human PSCs (Brown et al., 2014; Butts et al., 2017). In comparison with these studies, which focused on single populations, the advantage of our condition is that multiple ventral progenitor domains can be orderly induced in a single 3D structure. Because little is known about the mechanism regulating the distribution of interneuron and motor neuron subclasses within the developing spinal cord, our approach will provide novel insights on the development, patterning and overall organization of human ventral spinal cord tissue.

Our approach mimics the core aspects of human spinal cord development, but it also comes with important limitations. First, it is difficult to induce entire spinal cord tissues that contain all domains ranging from the dorsal side to ventral side. Because our culture system cannot provide concentration gradients of small molecules in the culture medium, it is difficult to induce two organizing centers with opposing roles at the same time. To overcome this problem, sophisticated microfluidic culture systems might be necessary. Second, induced spinal cord-like tissues showed inverted organization, with the neural progenitor cells on the outside of the structure where they formed the apical side and differentiated neural cells on the inside of the structure. A similar inversion was observed in other hPSC-derived *in vitro* neural tissues (Sakaguchi et al., 2015; Muguruma et al., 2015; Kuwahara et al., 2015). The mechanism regulating apico-basal polarity remains to be clarified, however, because these inverted structures were seen only in human PSC-derived tissues, differences in species or PSC state (e.g. primed versus naive) should be considered as candidate causes. Third, it is difficult to caudalize the positional identity of the induced spinal cord-like tissues toward lumbosacral levels. This result is consistent with a previous study showing that GDF11 is necessary to activate lumbosacral HOX genes (Lippmann et al., 2015). Modifications of the protocol to promote further caudalize positional identity is being considered. Fourth, we could not observe a clear formation of motor columns. One of the reasons might be the fact that the specification of motor neuron columns is related to not only dorso-ventral patterning but also complex cross-interactions with HOX effectors (Dasen et al., 2008; Philippidou et al., 2012; Mendelsohn et al., 2017). Our future challenge will be the recapitulation of motor neuron column formation in 3D and proper formation and regulation of the R-C axis.

The spinal cord is an essential tissue that connects the brain with other parts of the body. Although early developmental processes associated with spinal cord formation have been well studied using chick and mouse embryos, it still remains to be clarified how these complex network systems are correctly constructed during human development. Recently, tissue generation using hPSCs has been rigorously studied, including *in vitro* models of human central nervous system development (Muguruma et al., 2015; Kadoshima et al., 2013; Jo et al., 2016; Sakaguchi et al., 2015; Kuwahara et al., 2015). A combination of our 3D model of human spinal cord tissue development with cutting-edge technologies will likely contribute to a better understanding of the mechanisms and core principles underlying human neuronal network formation, especially of the ascending somatosensory and descending corticospinal system.

MATERIALS AND METHODS

Maintenance culture of human iPSCs

This study was approved by the ethics committees of Kyoto University, Kyoto, Japan. Human iPSCs (1039A1, 1231A3 and 1383D6) were maintained and cultured as previously described (Nishimura et al., 2016). Briefly, hiPSCs were maintained on LN511-E8-coated dishes with StemFit medium (Ajinomoto). For each passage, the cells were dissociated to single cells with Accutax (Innovative Cell Technologies) and replated at a density 1.3×10^4 cells into each well of a six-well plate.

Maintenance culture of hESCs

Human ESCs (KhES-1) were used in accordance with 'The Guidelines for Derivation and Utilization of Human Embryonic Stem Cells' of the Ministry of Education, Culture, Sports, Science and Technology of Japan after approval by the Institutional Review Board. hESCs were maintained and cultured as previously described (Sakaguchi et al., 2015). In brief, hESCs were maintained on a feeder layer of mouse embryonic fibroblasts inactivated by mitomycin C treatment in DMEM/F12 (Wako) supplemented with 20% knockout serum replacement (KSR, Invitrogen), 2 mM glutamine, 0.1 mM nonessential amino acids (Invitrogen), 5 ng ml⁻¹ recombinant human basic fibroblast growth factor (bFGF) (Wako) and 0.1 mM 2-mercaptoethanol under 2% CO₂. For passaging, hESC colonies were detached and recovered en bloc from the feeder layer by treating them with 0.25% (weight/vol) trypsin and 1 mg ml⁻¹ collagenase IV in PBS containing 20% (vol/vol) KSR and 1 mM CaCl₂ at 37°C for 7-8 min. The detached hESC clumps were broken into smaller pieces (several dozens of cells) by gentle pipetting. The passages were performed at a 1:4 to 1:6 split ratio every 4-5 days.

Differentiation culture of human iPSCs

The differentiation culture for spinal motor neurons (SMN protocol) was performed as described previously (Maury et al., 2015). Human iPSCs were dissociated to single cells using Accutax and quickly reaggregated using low cell adhesion U-bottomed 96-well plates (Lipidure-Coat Plate A96-U, NOF corporation) in differentiation medium (9000 cells per well, 100 µl). The differentiation medium was N2B27 [DMEM/F-12 (Wako), neurobasal medium (Gibco) (1:1), 0.5% (vol/vol) N2 supplement (ThermoFisher) and 1% (vol/vol) B27 supplement without vitamin A (Invitrogen)] supplemented with 1 mM L-glutamine (L-Glu, Sigma-Aldrich), 0.1 mM 2-mercaptoethanol (2-ME, Wako) and 0.5 µM ascorbic acid (Towa). Half the medium was changed once every 3 days. Defining the day on which the differentiation culture was started as day 0, 10 µM Y-27632 (Wako), 20 ng ml⁻¹ recombinant human basic fibroblast growth factor (bFGF, Wako) and 3 µM CHIR99021 (Stemgent) were added from day 0 to day 3, and 10 µM SB431542 (Tocris) and 0.2 µM LDN193189 (Stemgent) were added from day 0 to day 6. Retinoic acid (RA, 100 nM, Sigma-Aldrich) and 500 nM Smoothened agonist (SAG, Enzo) were added from day 3 to day 15.

For the induction of spinal cord tissues (3-DiSC condition), LDN193189 and SAG were removed from the SMN condition, and 10% (vol/vol) knockout serum replacement (KSR, Invitrogen) was added to the differentiation medium. Half the medium was changed once every 3 days. As for the differentiation culture of 1383D6, CHIR99021 treatment was reduced to 1.5 µM. As for the differentiation culture of Kh1, bFGF 20 ng ml⁻¹ and 50 µM Y-27632 were added to the differentiation medium for the first 3 days. After day 3, the same differentiation protocol used for human iPSCs was applied.

On day 15, the floating aggregates were transferred from a 96-well plate to a 6 cm Petri dish (non-cell adhesive) and further cultured in suspension with N2B27 medium supplemented with 1 mM L-Glu, 0.1 mM 2-ME, 0.5 µM ascorbic acid, 10 ng ml⁻¹ BDNF (Wako), 20 ng ml⁻¹ GDNF (Wako) and 100 nM RA.

For dorsalization, 15 ng ml⁻¹ BMP4 (R&D) was added from day 15 to day 24 (Fig. 2A). For ventralization, 50 nM or 500 nM SAG was added from day 3 to day 15 (Fig. 3A). For the inhibition of Notch signaling, 1 µM DAPT (Sigma-Aldrich) was added from day 15 to day 24 (Fig. 4B).

Neuronal dissociation culture

Neuronal dissociation culture was performed as previously described (Sakaguchi et al., 2015). The aggregates were dissociated to single cells

using the neural tissue dissociation kit (Sumitomo Bekelite, MB-X9901) on days 32–48 and plated onto poly-D-lysine/laminin/fibronectin-coated 2-well glass dishes at a density of 500,000 cells per well in neurobasal medium supplemented with 2% (vol/vol) B-27 supplement without vitamin A, 2 mM L-glutamine (Invitrogen), 10 ng ml⁻¹ BDNF and 20 ng ml⁻¹ GDNF. The medium was changed every 3 days.

Histological study of mouse embryonic spinal cord

The experiments were performed according to the Guidelines for Animal Experiment of Kyoto University, the Guide for the Care and Use of Laboratory Animals of the Institute for Laboratory Animal Resources (Washington, DC, USA), and the Animal Research: Reporting *in vivo* Experiments (The ARRIVE guidelines). Histological studies of mouse embryonic tissues were performed as previously described (Samata et al., 2016). Pregnant mice (C57BL/6NcrSlc) were obtained from Shimizu Laboratory Supplies (Kyoto, Japan). E11.5 embryos were removed and fixed in 4% paraformaldehyde (4°C, 2 h). Following cryostat sectioning, the cervical spinal cord was assessed using IHC.

Immunohistochemistry

IHC was performed as previously reported (Sakaguchi et al., 2015). In brief, aggregates were fixed in 4% paraformaldehyde, frozen in optimum cutting temperature (OCT) embedding medium and sectioned at 10 µm using a cryostat microtome. Serial sections of aggregates were attached onto slide glasses and incubated with primary antibodies (at 4°C overnight) following incubation with secondary antibodies conjugated with Alexa 488, 594 and 647 (at room temperature for 2 h). For the detection of GABA, 0.05% glutaraldehyde (Nacalai Tesque) was included in the fixative. All images were obtained using a confocal laser microscope (Olympus FV1000), except for wide-field images, which were obtained using a BioRevo fluorescence microscope (BZ-X710 Keyence). The primary antibodies used and their dilutions are listed in Table S1.

Quantitative analysis of immunohistochemistry

For quantitative analysis of IHC, nine aggregates from three independent culture experiments were examined. Cell counting was performed using ImageJ. Regarding Fig. 3R, the number of Brn3a⁺/Lhx9⁺ (dI1), Brn3a⁺/Lhx1⁺ (dI2), Brn3a⁺/Islet1⁺ (dI3), PAX2⁺/Lhx2⁺ (dI4) and DAPI⁺ cells were counted in two high-magnification field images covering one side of each aggregate. The percentage of individual neuronal types among total DAPI⁺ cells were calculated. For Fig. 5K, Chx10⁺ (V2a) and GATA3⁺ (V2b) cells were counted in one representative high-magnification field image of each aggregate. The percentage of each individual neuronal type among total V2 interneurons (V2a+V2b) was calculated.

Quantitative PCR

qPCR was performed as previously described (Nishimura et al., 2016). Each total RNA sample was extracted from 8–12 aggregates using RNeasy Plus Mini Kit (Qiagen), after which 1 µg of total RNA was used for reverse transcription by Super Script III First-Strand Synthesis System with Olig(dT)₂₀ primer (Invitrogen). Amplification was performed with Power SYBR Green PCR Master Mix (ThermoFisher). qPCR was performed on a StepOne detection system (Applied Biosystems). The data were normalized to GAPDH expression. Primer sequences are listed in Table S2.

For quantitative analysis, three independent differentiation culture experiments were performed. One or more total RNA samples were prepared in each differentiation experiment. For Fig. 1H, six total RNA samples from three independent culture experiments were examined. For Fig. 3C, seven total RNA samples from three independent culture experiments were examined. For Fig. 4C–E, seven total RNA samples from three independent culture experiments were examined. For Fig. S7C,D, five total RNA samples from three independent culture experiments were examined.

Bright field view time-lapse imaging of cell aggregation

The differentiation culture of hPSCs was performed as aforementioned with U-bottomed conical wells (Sumilon PrimeSurface plate;

Sumitomo Bakelite) under 3-DiSC condition. The original imaging data were taken by IncuCyte S3 Spheroid Software Module (Essen Bioscience) every 2 h for 66 h from the start of differentiation. Images were processed by WCIF ImageJ software and Adobe Premiere Pro CC 2017.

Statistical analysis

All data are shown as the mean±s.e.m. Statistical tests were performed with PRISM software (GraphPad version 5). For single comparisons, the statistical significance was tested by unpaired *t*-test or unpaired *t*-test with Welch's correction. For multiple comparisons, statistical significance was determined by one-way analysis of variance followed by Tukey's post hoc test.

Acknowledgement

We thank Dr Cantas Alev and Dr Makoto Ikeya for invaluable comments and helpful discussions, Dr Peter Karagiannis for critical reading of the manuscript, Dr Makoto Motono for technical advice on the hPSC culture, and Dr Sadaharu Torikoshi and Dr Yulius Hermanto for their technical assistance. H.S. is grateful to Dr Momoko Watanabe for invaluable comments.

Competing interests

The authors declare no competing or financial interests.

Author contributions

Conceptualization: T.O., H.S.; Methodology: T.O., H.S.; Validation: T.O.; Formal analysis: T.O., H.S.; Investigation: T.O.; Writing - original draft: T.O., H.S.; Writing - review & editing: S.M., J.T.; Supervision: H.S., S.M., J.T.; Project administration: H.S., J.T.; Funding acquisition: H.S., J.T.

Funding

This work was supported by a grant from the Network Program for Realization of Regenerative Medicine from the Japan Agency for Medical Research and Development (AMED) (18bm0204004h0006 to J.T.) and a Grant-in-Aid for Scientific Research from the Japan Society for the Promotion of Science (JSPS) (17H04302 to J.T., 18K15046 to H.S. and 16H06897 to H.S.). Deposited in PMC for immediate release.

Supplementary information

Supplementary information available online at <http://dev.biologists.org/lookup/doi/10.1242/dev.162214.supplemental>

References

- Alaynick, W. A., Jessell, T. M. and Pfaff, S. L. (2011). SnapShot: spinal cord development snapshot: spinal cord development. *Cell* **146**, 178–178.e1.
- Amoroso, M. W., Croft, G. F., Williams, D. J., O'Keeffe, S., Carrasco, M. A., Davis, A. R., Roybon, L., Oakley, D. H., Maniatis, T., Henderson, C. E. et al. (2013). Accelerated high-yield generation of limb-innervating motor neurons from human stem cells. *J. Neurosci.* **33**, 574–586.
- Benito-Gonzalez, A. and Alvarez, F. J. (2012). Renshaw cells and Ia inhibitory interneurons are generated at different times from p1 progenitors and differentiate shortly after exiting the cell cycle. *J. Neurosci.* **32**, 1156–1170.
- Bikoff, J. B., Gabitto, M. I., Rivard, A. F., Drobac, E., Machado, T. A., Miri, A., Brenner-Morton, S., Famojure, E., Diaz, C., Alvarez, F. J. et al. (2016). Spinal inhibitory interneuron diversity delineates variant motor microcircuits. *Cell* **165**, 207–219.
- Borowska, J., Jones, C. T., Zhang, H., Blacklaws, J., Goulding, M. and Zhang, Y. (2013). Functional subpopulations of V3 interneurons in the mature mouse spinal cord. *J. Neurosci.* **33**, 18553–18565.
- Brown, C. R., Butts, J. C., McCreedy, D. A. and Sakiyama-elbert, S. E. (2014). Generation of V2a interneurons from mouse embryonic stem cells. *Stem Cells Dev.* **23**, 1765–1776.
- Butts, J. C., McCreedy, D. A., Martinez-Vargas, J. A., Mendoza-Camacho, F. N., Hookway, T. A., Gifford, C. A., Taneja, P., Noble-Haesuslein, L. and McDevitt, T. C. (2017). Differentiation of V2a interneurons from human pluripotent stem cells. *Proc. Natl. Acad. Sci. USA* **114**, 4969–4974.
- Chizhikov, V. V. and Millen, K. J. (2004a). Control of roof plate formation by Lmx1a in the developing spinal cord. *Development* **131**, 2693–2705.
- Chizhikov, V. V. and Millen, K. J. (2004b). Mechanisms of roof plate formation in the vertebrate CNS. *Nat. Rev. Neurosci.* **5**, 808–812.
- Chizhikov, V. V. and Millen, K. J. (2005). Roof plate-dependent patterning of the vertebrate dorsal central nervous system. *Dev. Biol.* **277**, 287–295.
- Cho, G., Lim, Y., Cho, I.-T., Simonet, J. C. and Golden, J. A. (2014). Arx together with FoxA2, regulates Shh floor plate expression. *Dev. Biol.* **393**, 137–148.
- Dasen, J. S., De Camilli, A., Wang, B., Tucker, P. W. and Jessell, T. M. (2008). Hox repertoires for motor neuron diversity and connectivity gated by a single accessory factor, FoxP1. *Cell* **134**, 304–316.

- Du, Z.-W., Chen, H., Liu, H., Lu, J., Qian, K., Huang, C. T.-L., Zhong, X., Fan, F. and Zhang, S.-C. (2015). Generation and expansion of highly pure motor neuron progenitors from human pluripotent stem cells. *Nat. Commun.* **6**, 6626.
- Duval, N., Daubas, P., Bourcier de Carbon, C., St Cloment, C., Tinevez, J.-Y., Lopes, M., Ribes, V. and Robert, B. (2014). Msx1 and Msx2 act as essential activators of Atoh1 expression in the murine spinal cord. *Development* **141**, 1726-1736.
- Eiraku, M., Watanabe, K., Matsuo-Takasaka, M., Kawada, M., Yonemura, S., Matsumura, M., Wataya, T., Nishiyama, A., Muguruma, K. and Sasai, Y. (2008). Self-organized formation of polarized cortical tissues from ESCs and its active manipulation by extrinsic signals. *Cell Stem Cell* **3**, 519-532.
- Goulding, M. (2009). Circuits controlling vertebrate locomotion: moving in a new direction. *Nat. Rev. Neurosci.* **10**, 507-518.
- Gross, M. K., Dottori, M. and Goulding, M. (2002). Lbx1 specifies somatosensory association interneurons in the dorsal spinal cord. *Neuron* **34**, 535-549.
- Gupta, S., Sivalingam, D., Hain, S., Makkar, C., Sosa, E., Clark, A. and Butler, S. J. (2018). Deriving dorsal spinal sensory interneurons from human pluripotent stem cells. *Stem Cell Reports* **10**, 390-405.
- Jessell, T. M. (2000). Neuronal specification in the spinal cord: inductive signals and transcriptional codes. *Nat. Rev. Genet.* **1**, 20-29.
- Jo, J., Xiao, Y., Sun, A. X., Cukuroglu, E., Tran, H.-D., Göke, J., Tan, Z. Y., Saw, T. Y., Tan, C.-P., Lokman, H. et al. (2016). Midbrain-like organoids from human pluripotent stem cells contain functional dopaminergic and neuromelanin-producing neurons. *Cell Stem Cell* **19**, 248-257.
- Joshi, K., Lee, S., Lee, B., Lee, J. W. and Lee, S.-K. (2009). LMO4 controls the balance between excitatory and inhibitory spinal V2 interneurons. *Neuron* **61**, 839-851.
- Kadoshima, T., Sakaguchi, H., Nakano, T., Soen, M., Ando, S., Eiraku, M. and Sasai, Y. (2013). Self-organization of axial polarity, inside-out layer pattern, and species-specific progenitor dynamics in human ES cell-derived neocortex. *Proc. Natl. Acad. Sci. USA* **110**, 20284-20289.
- Kuwahara, A., Ozone, C., Nakano, T., Saito, K., Eiraku, M. and Sasai, Y. (2015). Generation of a ciliary margin-like stem cell niche from self-organizing human retinal tissue. *Nat. Commun.* **6**, 6286.
- Le Dreau, G., Garcia-Campmany, L., Rabadan, M. A., Ferronha, T., Tozer, S., Briscoe, J. and Marti, E. (2012). Canonical BMP7 activity is required for the generation of discrete neuronal populations in the dorsal spinal cord. *Development* **139**, 259-268.
- Lee, K. J., Dietrich, P. and Jessell, T. M. (2000). Genetic ablation reveals that the roof plate is essential for dorsal interneuron specification. *Nature* **403**, 734-740.
- Lippmann, E. S., Williams, C. E., Ruhl, D. A., Estevez-Silva, M. C., Chapman, E. R., Coon, J. J. and Ashton, R. S. (2015). Deterministic HOX patterning in human pluripotent stem cell-derived neuroectoderm. *Stem Cell Reports* **4**, 632-644.
- Liu, Y., Helms, A. W. and Johnson, J. E. (2004). Distinct activities of Msx1 and Msx3 in dorsal neural tube development. *Development* **131**, 1017-1028.
- Lu, D. C., Niu, T. and Alaynick, W. A. (2015). Molecular and cellular development of spinal cord locomotor circuitry. *Front. Mol. Neurosci.* **8**, 25.
- Mansour, A. A., Khazanov-Zisman, S., Netser, Y., Klar, A. and Ben-Arie, N. (2014). Noto3 plays an integral role in dorsoventral patterning of the spinal cord by segregating floor plate/p3 fates via Nkx2.2 suppression and Foxa2 maintenance. *Development* **141**, 574-584.
- Maury, Y., Côme, J., Piskrowski, R. A., Salah-Mohellibi, N., Chevalere, V., Peschanski, M., Martinat, C. and Nedelec, S. (2015). Combinatorial analysis of developmental cues efficiently converts human pluripotent stem cells into multiple neuronal subtypes. *Nat. Biotechnol.* **33**, 89-96.
- Mazzoni, E. O., Mahony, S., Peljto, M., Patel, T., Thornton, S. R., McCuine, S., Reeder, C., Boyer, L. A., Young, R. A., Gifford, D. K. et al. (2013). Saltatory remodeling of Hox chromatin in response to rostrocaudal patterning signals. *Nat. Neurosci.* **16**, 1191-1198.
- Meinhardt, A., Eberle, D., Tazaki, A., Ranga, A., Niesche, M., Wilsch-Bräuninger, M., Stec, A., Schackert, G., Lutolf, M. and Tanaka, E. M. (2014). 3D reconstitution of the patterned neural tube from embryonic stem cells. *Stem Cell Reports* **3**, 987-999.
- Mendelsohn, A. I., Dasen, J. S. and Jessell, T. M. (2017). Divergent Hox coding and evasion of retinoid signaling specifies motor neurons innervating digit muscles. *Neuron* **93**, 792-805.e4.
- Muguruma, K., Nishiyama, A., Kawakami, H., Hashimoto, K. and Sasai, Y. (2015). Self-organization of polarized cerebellar tissue in 3D culture of human pluripotent stem cells. *Cell Rep.* **10**, 537-550.
- Müller, T., Brohmann, H., Pierani, A., Heppenstall, P. A., Lewin, G. R., Jessell, T. M. and Birchmeier, C. (2002). The homeodomain factor *lhx1* distinguishes two major programs of neuronal differentiation in the dorsal spinal cord. *Neuron* **34**, 551-562.
- Nishimura, K., Doi, D., Samata, B., Murayama, S., Tahara, T., Onoe, H. and Takahashi, J. (2016). Estradiol facilitates functional integration of iPSC-derived dopaminergic neurons into striatal neuronal circuits via activation of integrin $\alpha 5 \beta 1$. *Stem Cell Reports* **6**, 511-524.
- Novitsch, B. G., Wichterle, H., Jessell, T. M. and Sockanathan, S. (2003). A requirement for retinoic acid-mediated transcriptional activation in ventral neural patterning and motor neuron specification. *Neuron* **40**, 81-95.
- Peljto, M., Dasen, J. S., Mazzoni, E. O., Jessell, T. M. and Wichterle, H. (2010). Functional diversity of ESC-derived motor neuron subtypes revealed through intraspinal transplantation. *Cell Stem Cell* **7**, 355-366.
- Philippidou, P. and Dasen, J. S. (2013). Hox genes: choreographers in neural development, architects of circuit organization. *Neuron* **80**, 12-34.
- Philippidou, P., Walsh, C. M., Aubin, J., Jeannotte, L. and Dasen, J. S. (2012). Sustained Hox5 gene activity is required for respiratory motor neuron development. *Nat. Neurosci.* **15**, 1636-1644.
- Ranga, A., Girgin, M., Meinhardt, A., Eberle, D., Caiazzo, M., Tanaka, E. M. and Lutolf, M. P. (2016). Neural tube morphogenesis in synthetic 3D microenvironments. *Proc. Natl. Acad. Sci. USA* **113**, E6831-E6839.
- Ribes, V. and Briscoe, J. (2009). Establishing and interpreting graded sonic hedgehog signaling during vertebrate neural tube patterning: the role of negative feedback. *Cold Spring Harb. Perspect. Biol.* **1**, a002014-a002014.
- Ribes, V., Balaskas, N., Sasai, N., Cruz, C., Dessaud, E., Cayuso, J., Tozer, S., Yang, L. L., Novitsch, B., Marti, E. et al. (2010). Distinct Sonic Hedgehog signaling dynamics specify floor plate and ventral neuronal progenitors in the vertebrate neural tube. *Genes Dev.* **24**, 1186-1200.
- Sakaguchi, H., Kadoshima, T., Soen, M., Narii, N., Ishida, Y., Ohgushi, M., Takahashi, J., Eiraku, M. and Sasai, Y. (2015). Generation of functional hippocampal neurons from self-organizing human embryonic stem cell-derived dorsomedial telencephalic tissue. *Nat. Commun.* **6**, 8896.
- Samata, B., Doi, D., Nishimura, K., Kikuchi, T., Watanabe, A., Sakamoto, Y., Kakuta, J., Ono, Y. and Takahashi, J. (2016). Purification of functional human ES and iPSC-derived midbrain dopaminergic progenitors using LRTM1. *Nat. Commun.* **7**, 13097.
- Stam, F. J., Hendricks, T. J., Zhang, J., Geiman, E. J., Francius, C., Labosky, P. A., Clotman, F. and Goulding, M. (2012). Renshaw cell interneuron specialization is controlled by a temporally restricted transcription factor program. *Development* **139**, 179-190.
- Timmer, J. R., Wang, C. and Niswander, L. (2002). BMP signaling patterns the dorsal and intermediate neural tube via regulation of homeobox and helix-loop-helix transcription factors. *Development* **129**, 2459-2472.

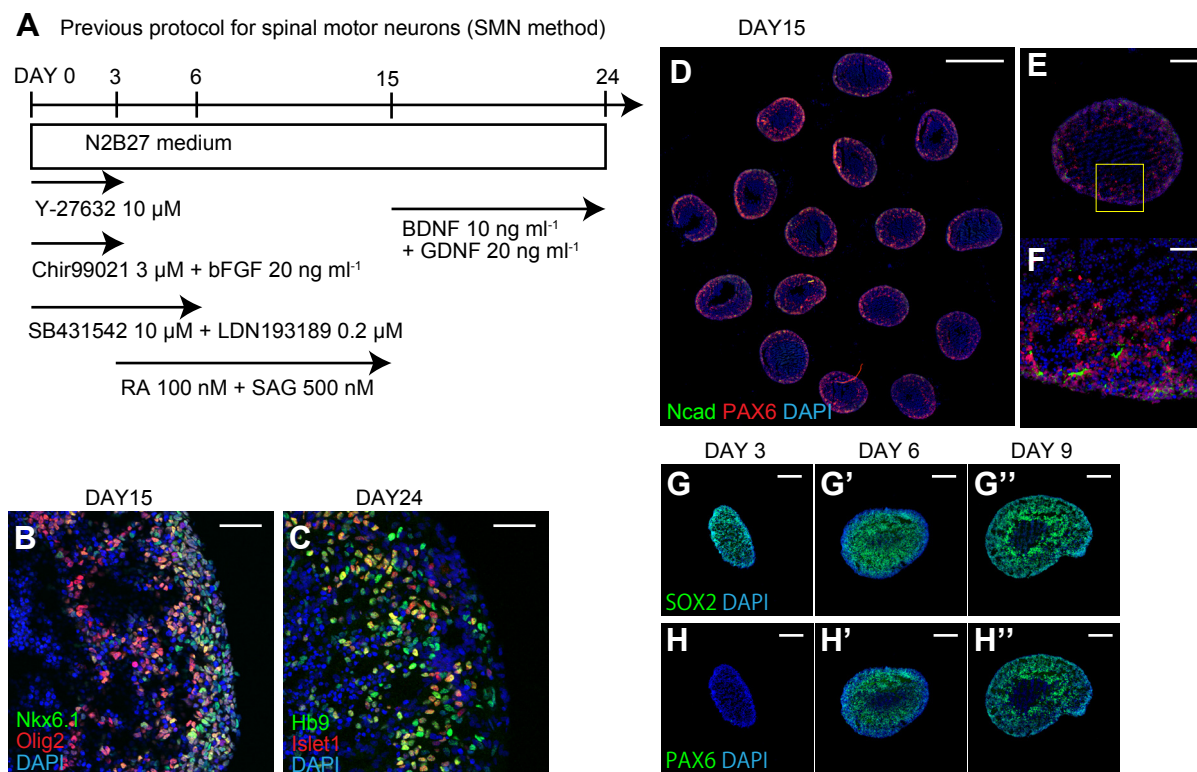


Fig. S1 Generation of spinal motor neurons using a previously described protocol.

(A) Schematic of the differentiation protocol for spinal motor neurons (SMN protocol). (B) Nkx6.1⁺/Olig2⁺ spinal motor neuron progenitors were efficiently generated on day 15. (C) Hb9⁺/Islet1⁺ spinal motor neuron precursors were efficiently generated on day 24. (D-F) The expression of N-cadherin was observed in a discontinuous manner. (G-H'') SOX2⁺/PAX6⁺ rosette-like structure formation was observed up to day 9. Scale bars: 1000 μm (D); 200 μm (E, G-H''); 50 μm (B, C, F).

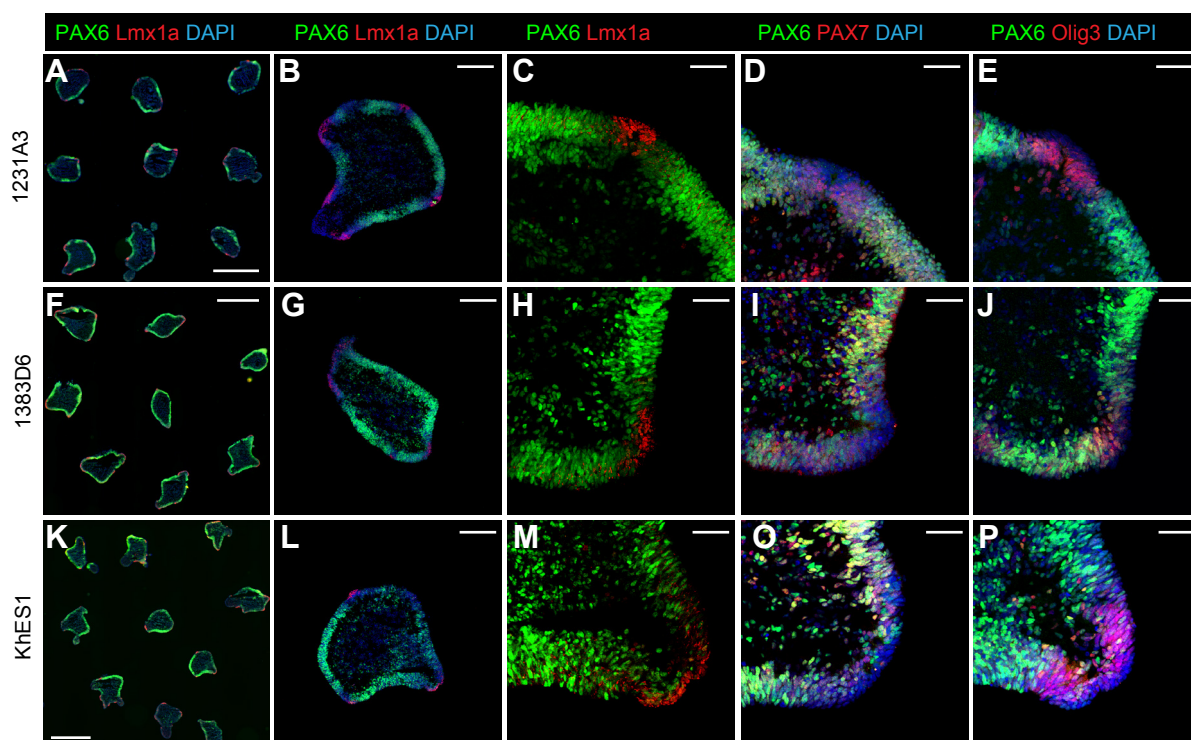


Fig. S2 Induction of dorsal spinal cord-like tissues from other hPSC lines. Dorsal spinal cord-like tissues could be induced using other human iPS cell lines (1231A1 (A-E), 1383D6 (F-J)) and a human ES cell line (KhES1 (K-P)). Continuous epithelium structure expressed PAX6 (A, E, I). Lmx1a⁺ domains were induced in PAX6⁻ regions (A-C, F-H, K-M). PAX6⁺ continuous epithelium co-expressed PAX7 (D, I, Q). Olig3⁺ domains were induced adjacent to Lmx1a⁺ regions (E, J, P). These structures were observed in 90.9% (1231A3), 83.3% (1383D6) and 57.5% (KhES1) of the analyzed aggregates in 3 independent experiments. Scale bars: 1000 μ m (A, F, K); 200 μ m (B, G, L); 50 μ m (C-E, H-J, M-P).

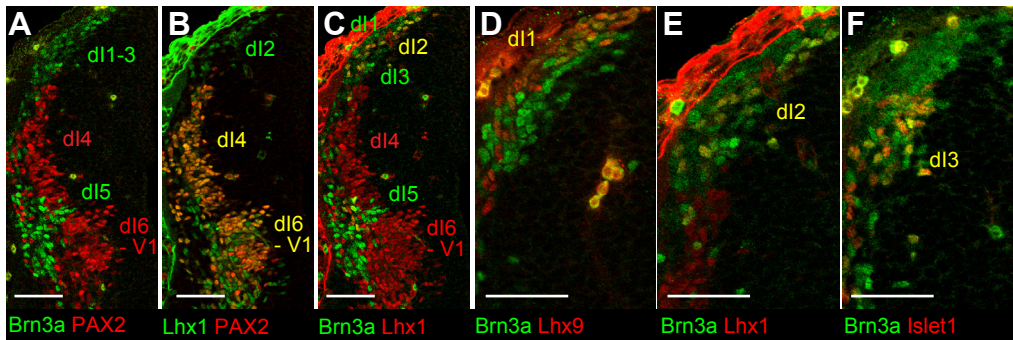


Fig. S3. Expression pattern of dorsal interneuron markers in mouse embryo E11.5. (A) Brn3a⁺ population and PAX2⁺ population exhibited separate distributions. (B) Lhx1⁺/PAX2⁺ population was observed in the dorsal side and ventral side. (C) Lhx1⁺ cells in the dorsal side co-expressed Brn3a. (D-F) Among Brn3a⁺ cells, Lhx9⁺ cells (D), Lhx1⁺ cells (E), and Islet1⁺ cells (F) were dl1, dl2 and dl3, respectively. Scale bars:100 μ m (A-C); 50 μ m (D-F).

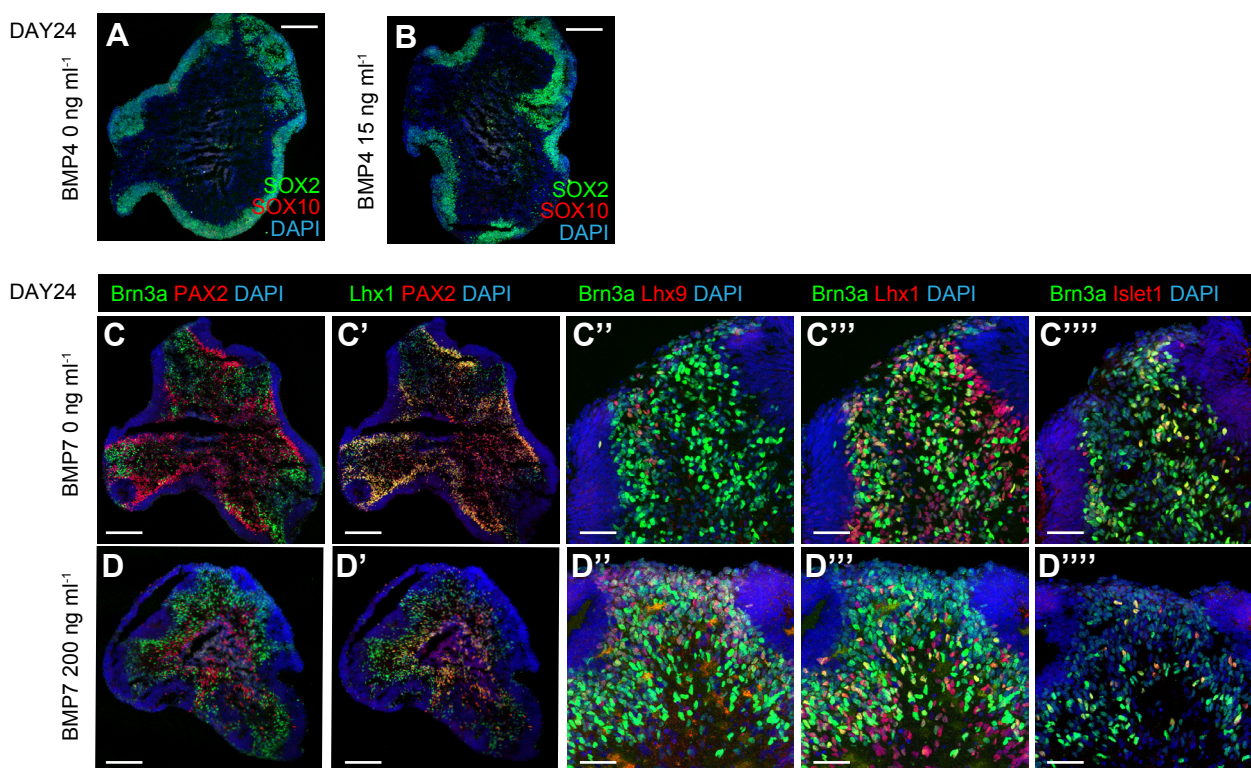


Fig. S4. BMP treatment dorsalized the identity of spinal cord-like tissues.

(A, B) Immunostaining for SOX2 and SOX10 on day 24 under BMP4 0 ng ml⁻¹ (A) and BMP4 15 ng ml⁻¹ (B). SOX2 was expressed in the epithelial structure, but SOX10⁺ cells were rarely detected in (A). BMP4 treatment did not increase SOX10⁺ cells. (C-C'''') Immunostaining under BMP7 0 ng ml⁻¹ on day 24. (C) Brn3a⁺ and PAX2⁺ cell populations were detected. (C') PAX2⁺ populations co-expressed Lhx1, suggesting the generation of dl4 or dl6. (C'' -C'''') Lhx9⁺/Brn3a⁺, Lhx1⁺/Brn3a⁺, Islet1⁺/Brn3a⁺ populations were detected, suggesting the generation of dl1, dl2 and dl3 respectively. (D-D'''') Immunostaining under BMP7 200 ng ml⁻¹ on day 24. (D) Brn3a⁺ populations were mainly generated. (D') PAX2⁺/Lhx1⁺ (dl4/6) cells were decreased compared with BMP7 0 ng ml⁻¹. (D'' -D'''') Lhx9⁺/Brn3a⁺ (dl1), Lhx1⁺/Brn3a⁺ (dl2) cells were mainly generated, while only a few number of Islet1⁺/Brn3a⁺ (dl3) cells were detected. Scale bars: 200 μ m (A, B, C, C' , D, D'); 50 μ m (C'' -C'''' , D'' -D'''').

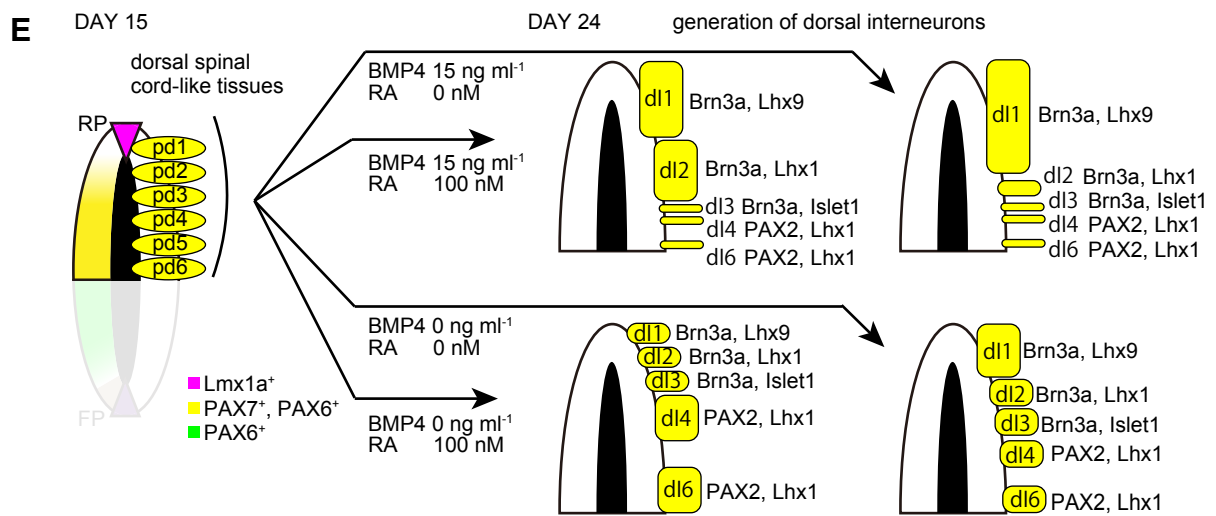
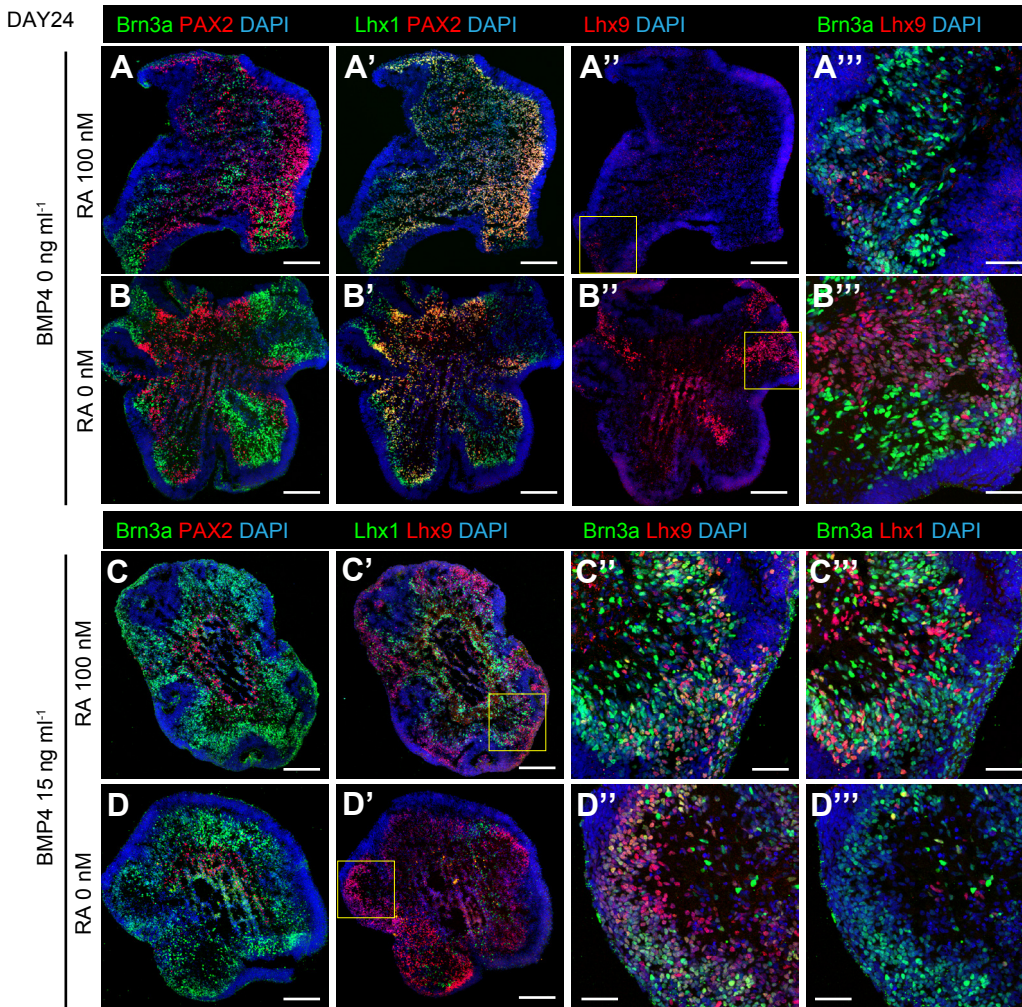


Fig. S5. Examination of the interplay between BMPs and RA

(A, B) The role of RA between days 15 and 24 were examined under BMP4 0 ng ml⁻¹ condition. (A-A''') Immunostaining under RA 100 nM on day 24. (A) Brn3a⁺ and PAX2⁺ cell populations were generated. (A') PAX2⁺ populations co-expressed Lhx1, suggesting the generation of dl4 or dl6. (A'', A''') Lhx9⁺/Brn3a⁺ cells were detected, suggesting the generation of dl1. (B-B''') Immunostaining under RA 0 nM on day 24. (B, B') Compared with RA 100 nM, Brn3a⁺ cells were increased, while PAX2⁺/Lhx1⁺ (dl4/6) cells were decreased. (B'', B''') Lhx9⁺/Brn3a⁺ (dl1) cells were increased. (C, D) The role of RA between days 15 and 24 was examined under BMP4 15 ng ml⁻¹ condition. (C-C''') Immunostaining under RA 100 nM on day 24. (C) Brn3a⁺ cells were mainly generated, while few PAX2⁺ cells were observed. (C' -C''') Lhx9⁺/Brn3a⁺ (dl1) and Lhx1⁺/Brn3a⁺ (dl2) cells were generated. (D-D''') Immunostaining under RA 0 nM on day 24. (D) Brn3a⁺ cells were mainly generated. (D' -D''') Lhx9⁺/Brn3a⁺(dl1) cells were mainly generated, while few Lhx1⁺/Brn3a⁺ (dl2) cells were detected. (E) Schematic summary of the examined conditions. Scale bars: 200 μm (A-A'', B-B'', C, C', D, D'); 50 μm (A''', B''', C'', C''', D'', D''').

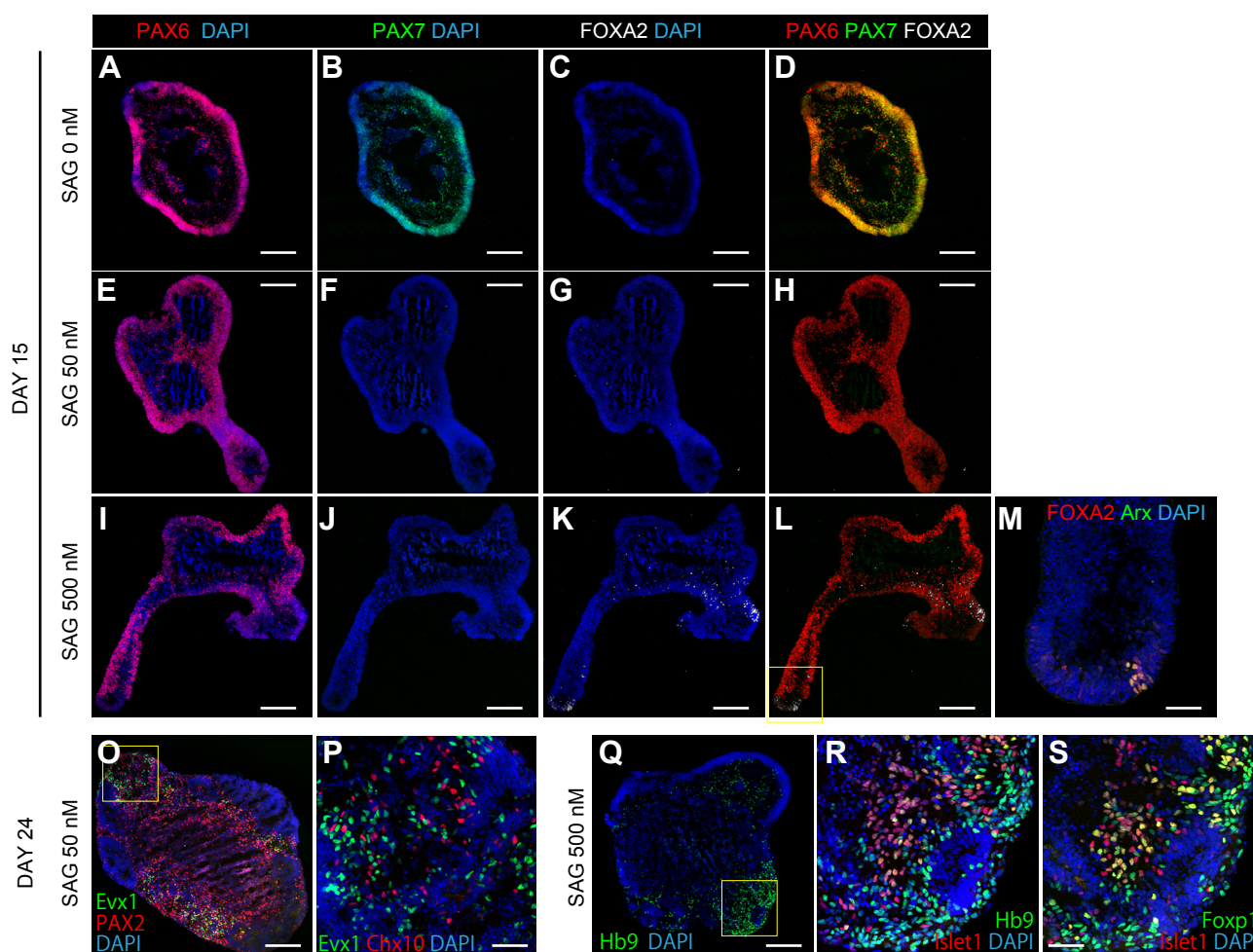


Fig. S6. Spinal cord-like tissues were ventralized by activating Shh signaling in a dose-dependent manner. (A-D) Under SAG 0 nM, continuous epithelium expressed both PAX6 (A) and PAX7 (B) but not FOXA2 (C, D). (E-H) Under SAG 50 nM, continuous epithelium expressed PAX6 (E), but not PAX7 (F) or FOXA2 (G, H). (I-L) Under SAG 500 nM, continuous epithelium partially expressed PAX6 (I), but not PAX7 (J). FOXA2 expression was also observed (K, L), suggesting the generation of the ventral-most part of the spinal cord. (M) Some of FOXA2⁺ cells co-expressed Arx, suggesting the presence of definitive floor plate. (O) Evx1⁺ cells were observed on day 24 under SAG 50 nM condition, suggesting the generation of V0. (P) Chx10⁺ cells were detected, suggesting the generation of V2a. (Q, R) Hb9⁺, Islet1⁺ and Hb9⁺/Islet1⁺ cells were generated on day 24 under SAG 500 nM condition. (R) FOXP1⁺ cells were observed, suggesting the generation of lateral motor column motor neurons. Scale bars: 200 μ m (A-L, O, Q); 50 μ m (M, P, R, S).

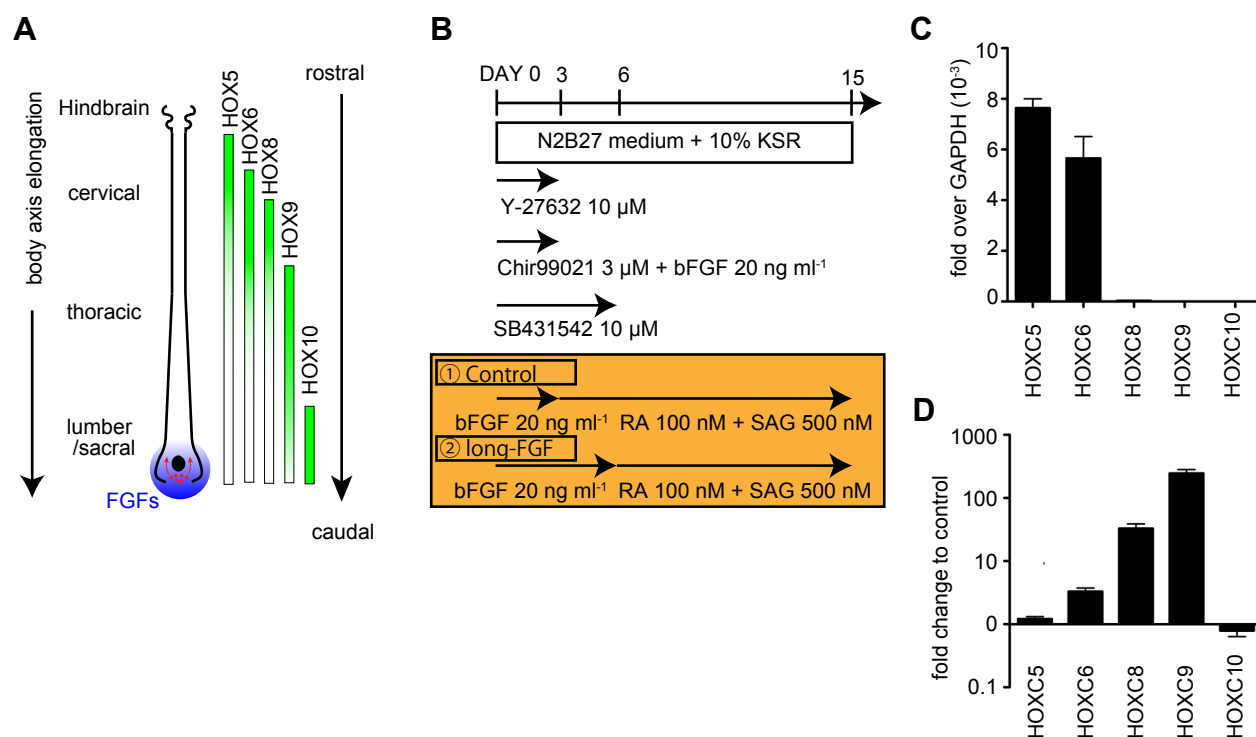


Fig. S7. Evaluation of positional identities along rostro-caudal axis. (A) Schematic showing the expression pattern of HOX gene along the R-C axis. (B) Schematic of the examined conditions. (C) qPCR analysis on day 15 showing the expression of HOX genes under control conditions (n=5 total RNA samples from 3 independent culture experiments) (D) qPCR analysis on day 15 showing the relative expression of HOX genes under long FGF treatment conditions compared to control conditions (n=5 total RNA samples from 3 independent culture experiments). HOXC8 and HOXC9 were upregulated, while HOXC10 was not. Each bar represents s.e.m.

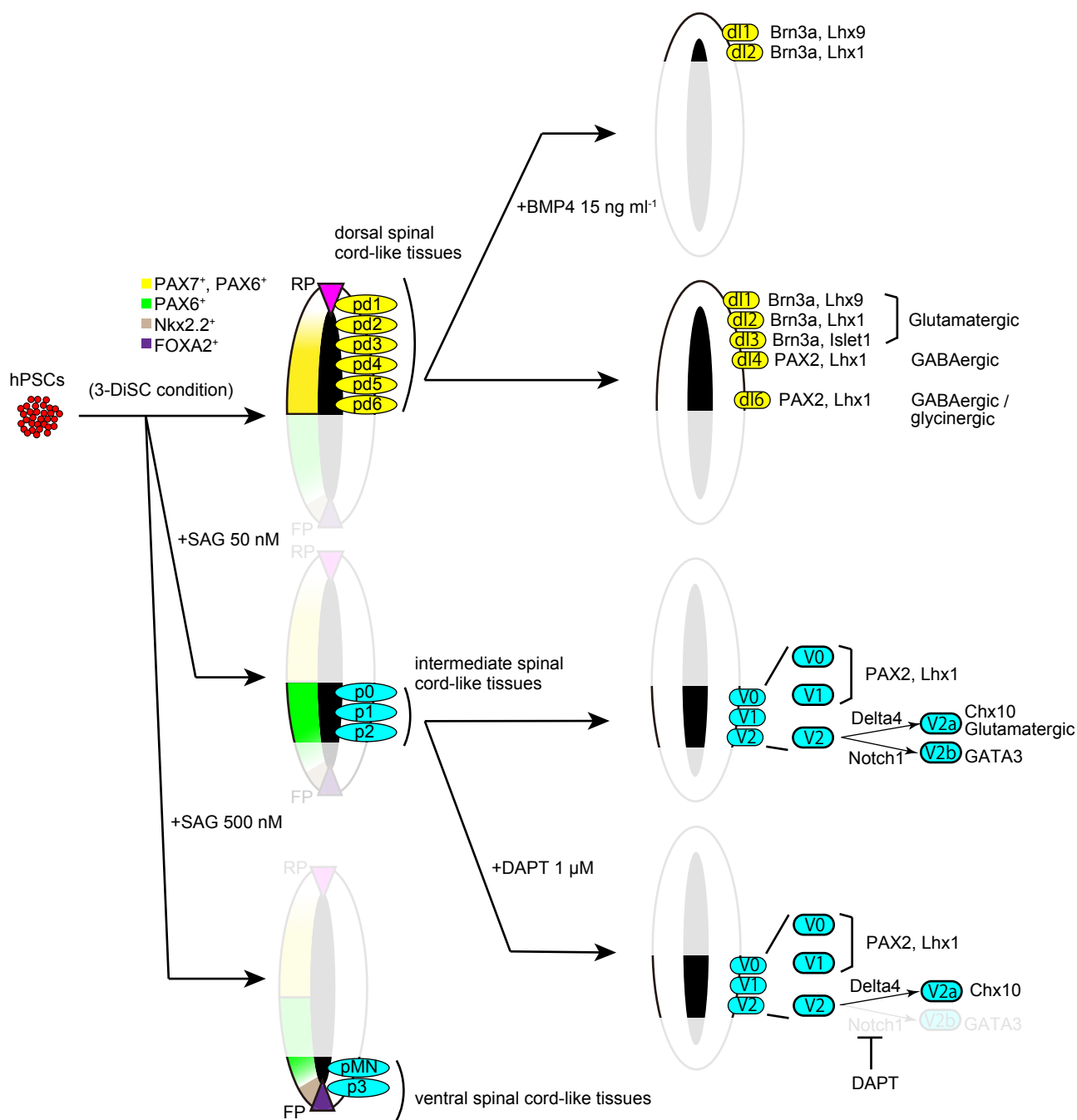


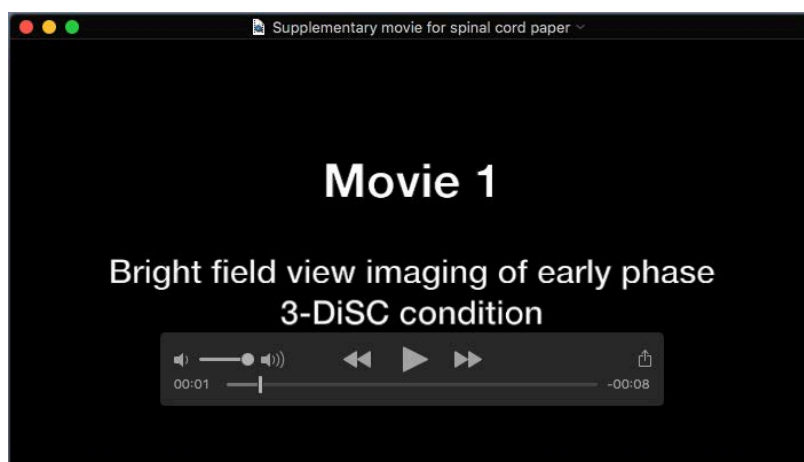
Fig. S8. Schematic summary of examined conditions for 3D spinal cord tissues.

Table. S1. List of primary antibodies and their dilutions for Immunostaining

Antibodies	Company	Catalog#	Host spices	Dilution
Arx	R&D	AF7068	Sheep	1:100
PKC ζ	SantaCruz	sc-216	Rabbit	1:100
Brachyury	R&D	AF2085	Goat	1:200
Brn3a	SantaCruz	sc-31984	Goat	1:250
Calbindin	Swant	D-28K	Mouse	1:1000
ChAT	Millipore	AB144P	Goat	1:200
Chx10	Santa Cruz	sc-21690	Goat	1:500
Dbx1	Sigma	HPA039802	Rabbit	1:100
Evx1	DSHB	99.1-3A2	Mouse	1:100
FOXA2	Santa Cruz	sc-6554	Goat	1:500
FOXP1	Abcam	ab32010	Mouse	1:500
FOXP2	Abcam	ab16046	Rabbit	1:4000
GABA	Millipore	MAB316	Mouse	1:250
GABA	Sigma	A2052	Rabbit	1:2000
GAD67	Millipore	MAB5406	Mouse	1:1000
GATA3	R&D	MAB6330	Mouse	1:500
GFAP	Santa Cruz	sc-6170	Goat	1:500
Hb9	DSHB	81.5C10	Mouse	1:100
Islet1	Sigma	HPA057416	Rabbit	1:500
Lhx1	DSHB	4F2	Mouse	1:100
Lhx9	Sigma	HPA009695	Rabbit	1:100
Lmx1a	Sigma	HPA030088	Rabbit	1:2000
MafB	Sigma	HPA005653	Rabbit	1:250
MSX1/2	DSHB	4G1	Mouse	1:200
N-cadherin	BD	610920	Mouse	1:1000
Nkx2.2	DSHB	74.5A5	Mouse	1:100
Nkx6.1	DSHB	F55A12	Mouse	1:100
Olig2	Millipore	AB9610	Rabbit	1:1000
Olig3	Sigma	HPA018303	Rabbit	1:100
PAX2	Covance	PRB-276P	Rabbit	1:500
PAX6	BD	561462	Mouse	1:500
PAX6	Covance	PRB-278P	Rabbit	1:500
PAX7	DSHB	PAX7	Mouse	1:100
phospho-SMAD1/5	Cell Signaling	9516	Rabbit	1:500
SOX1	R&D	AF3369	Goat	1:1000
SOX2	SantaCruz	sc-17320	Goat	1:500
SOX2	Abcam	ab97959	Rabbit	1:500
SOX10	Abcam	ab108408	Rabbit	1:500
Tuj1	Tuj1	MMS435P	Mouse	1:1000
Tuj1	Tuj1	PRB-435P	Rabbit	1:1000
Vglut2	R&D	MAB5504	Mouse	1:200
Vglut2	Synaptic Systems	135 404	Guinea Pig	1:1000
Wnt1	Abcam	ab15251	Rabbit	1:500

Table. S2. List of genes and their primer sequences for qPCR analysis

Gene	Forward (5' -3')	Reverse (5' -3')
Brn3a	CTCCCTGAGCACAAGTACCC	TGAAAGGATGGCTCTTGCCC
Dbx1	GTACATCAGCAAGCCCGACC	AGTTCCGCCATTTTCATGCGT
Dbx2	CCCAACAGCACTCAAGTCCA	AGCCCCAGTAAGTACACCCT
FOXA2	TTCAGGCCCGGCTAACTCT	AGTCTCGACCCCCACTTGCT
HOXC5	GAGGAGCGAGCTAAGAGCAG	GTGGCTCATGTGCAGTTTGG
HOXC6	ACAGACCTCAATCGCTCAGG	GTACCGCGAGTAGATCTGGC
HOXC8	CCTCCGCCAACACTAACAGT	AAACATGAGGCTGGGAGACG
HOXC9	CGTGGACTCGCTCATCTCTC	AAAATCGCTACAGTCCGGCA
HOXC10	AGTGACTTCAATTGCGGGGT	GATAGGTGTTGAGGGCGAGG
Lbx1	CGCCAGCAAGACGTTTAAG	CTGCCCAAAGATGGTCATAC
Lmx1a	TCAGAAGGGTGATGAGTTTGTCC	GGGGCGCTTATGGTCCTTG
Nkx2.2	AAACCATGTACGCGCTCA	GGCGTTGACTGCATGTGCT
Nkx6.1	CACACGAGACCCACTTTTTCC	CCCAACGAATAGGCCAAACG
Olig2	GGGCCACAAGTTAGTTGGAA	GAGGAACGGCCACAGTTCTA
Olig3	CCTGCTCGCCAGAACTACA	CCCCATAGATCTCGCCAACC
PAX6	TCTTTGCTTGGGAAATCCG	CTGCCCGTTCAACATCCTTAG
PAX7	CTTCAGTGGGAGGTCAGGTT	CAAACACAGCATCGACGG
GAPDH	GGTCGGAGTCAACGGATTG	TCAGCCTTGACGGTGCCATG



Movie 1. Bright field view imaging of early phase 3-DiSC condition

The original imaging data were taken by using the IncuCyte S3 Live Cell Imaging System every 2 hours for 66 hours during tissue differentiation under 3-DiSC condition. After seeding hPSCs to each well of a U-bottomed 96-well plate, a cell aggregate became obvious from 10 hours after the start of differentiation. Some cells were not included in the aggregate and remained around the aggregate. Scale bar: 400 μm .